Reprinted Report,
Updated: 13-09-2001,

Internet:
http://dutw189.wbmt.tudelft.nl/~johan
http://www.shipmotions.nl

Report 158S, March 1972,
Netherlands Ship Research Centre TNO,
Shipbuilding Department,
Leeghwaterstraat 5, Delft,
The Netherlands.
E-mail: J.M.J.Journee@wbmt.tudelft.nl

Prediction of Ship Manoeuvrability

G. van Leeuwen and J.M.J. Journée

Delft University of Technology

Summary

Static sway- and oscillatory yawing tests with a 1:55 model of the 50.000 DWT tanker "British Bombardier" are discussed.
The principal purpose of these tests was to determine the coefficients of a non-linear mathematical model to predict a number of standard manoeuvres, which were earlier performed with the full-scale ship before. Clarke (1965) describes the results of these full-scale manoeuvres.
The mathematical model chosen is based on the Abkowitz Taylor-expansion of the hydrodynamic forces and moments; see Abkowitz (1964). However, there is a principal difference with respect to the variables involved, which enables a more correct description of some non-linear phenomena. Comparison of the predicted manoeuvres with the corresponding full-scale data shows a rather good agreement.
For comparison purposes some experiments have been performed as well with a small model of the same tanker ($\alpha = 100$). However it is found that scale effects, due to the very low Reynolds number, have a considerable influence on the hydrodynamic derivatives. Some interesting additional figures are given showing the contributions of each term of the mathematical model during a turning circle manoeuvre while also the change of the stability roots during this manoeuvre is plotted.

1 Introduction

At the Delft Shipbuilding Laboratory model tests were performed to determine the coefficients of a non-linear mathematical model, which describes the still water manoeuvrability properties of a ship. Two types of tests are performed. First the static towing tests with a constant drift and rudder angle and second oscillation tests to determine the added mass effect in the swaying motion and the hydrodynamic derivatives of the yawing

motion. The main particulars of both ship and models are summarised in Table 1.

modelscale	1:1	1:55	1:100
L_{pp} (m)	220.980	4.018	2.210
beam (m)	29.566	.538	.296
draught (m)	12.497	.227	.125
volume displacement (m^3) (moulded)	65.089×10^3	.3912	.0651
diameter of propeller (m)	6.706	.122	.067
number of blades	5	5	5
$(H/D)_{.7\,R}$	.752	.752	.752
F_a/F	.608	.608	.608
longitudinal radius of gyration		.25 *L*	.25 *L*
rudder area (cm^2)	38.32×10^4	126.6	38.3

Table 1 Main Particulars of Ship and Models

The principal purpose of the tests is to obtain information on the possibility to predict the principal manoeuvres of a ship, using an adequate mathematical model and model experiments to determine the coefficients of this model. For comparison purposes, Clarke (1965) performed full-scale trials.

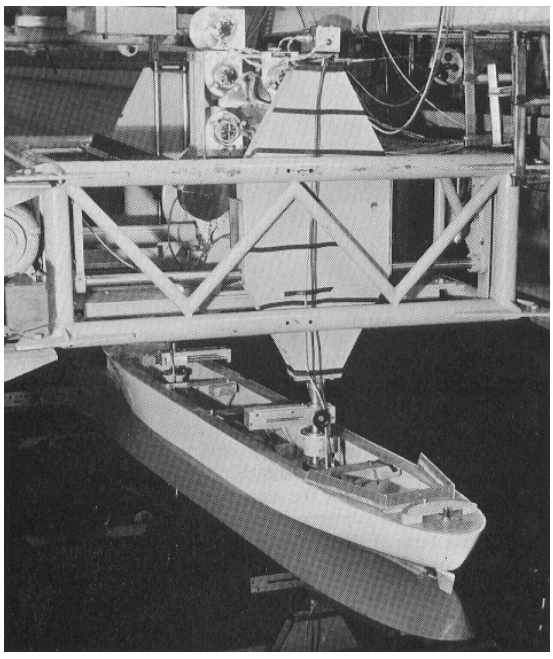

Figure 1 Ship Model under Oscillator in Towing Tank

The model experiments have been performed at four different initial speed conditions, corresponding with a constant propeller power each. Originally the results of these four sets of tests have been kept separated, because it was assumed that some of the non-dimensional coefficients could change with the Froude number, based on the initial speed. In that case a set of coefficients which would be different for each initial speed would have been found. Clarke (1965) gives the results of this tentative analysis.

During the analysis of the experimental data, it was found that the principal differences between some of the non-dimensional coefficients could be described effectively by considering the local water velocity near the rudder. In this way the apparent Froude-effect in these coefficients rather could be called a "power-effect" while the differences in the other coefficients were not considered significant, in view of both the available information and the accuracy of the measurements.

It is not to be expected however, that this method of describing the phenomena mentioned above will hold for other ships. Especially when the Froude number becomes high e.g. 0.30 or higher, it is not very likely that there will be no real Froude effect in some hydrodynamic derivatives if they are compared with the corresponding values found at a Froude number of 0.10 e.g.

Provided a certain mathematical model has been adopted, there are several methods to determine the coefficients of such a model by model tests. The main problem is to find out how far uncoupling of the three motions in the horizontal plane is allowed. Of course, during an actual manoeuvre the motions are always coupled and even if the mathematical model contains terms, which are meant to describe the cross-coupling effects one is not sure about the way these effects have to be determined. The most convenient method might be to perform free running model tests and find the

coefficients of the mathematical model by analysing the data concerning position and course of a number of representative manoeuvres. In that case all variables remain coupled in the natural way. In general however too less room is available for these kinds of manoeuvres, so that one is pressed to find an acceptable alternative. In this respect the forced horizontal oscillation test provides an alternative solution. On the other hand, the problem of uncoupling the motions as mentioned above is introduced. Another practical problem is to choose the right combinations of oscillator frequencies and amplitudes. Considering an actual oscillatory motion, due to the harmonic motion of the rudder, it is found that the combinations of frequencies and amplitudes involved in these motions cannot easily be simulated by horizontal oscillation tests. This is because the actual range of amplitudes is of the magnitude of one half to many ship lengths. In most towing tanks sufficient width is not available in this respect. These problems are considered in greater detail in by Van Leeuwen (1969a).

The conclusion is that most horizontal oscillation tests involve an unnatural relation of amplitudes and frequencies. In other words the ratios of velocity and acceleration amplitudes are quite different from the actual values. Apparently this is no problem, because most of the mathematical models which are now in use do not contain any cross-coupling terms between velocities and accelerations. This does not imply, however, that such cross-coupling effects could not be introduced, if the range of ratios of these variables is extended too far.

Some final remarks on the mathematical model.

In the course of the years a lot of studies were devoted to this subject, starting with Davidson and Schiff (1946), who described a model based on the linear equations of motion. This set of equations, which originally involves three equations, describing the surging, swaying and yawing motion, has been used by several authors, though unfortunately omitting the surge equation. Abkowitz (1964) has proposed one of the most extended non-linear mathematical models. In this model the hydrodynamic part of the forces is expanded into a Taylor series of the variables concerned. This principle is very useful, particularly if the constants of the model are to be determined by the analysis of forced model tests, because all imaginable hydrodynamic effects in principle can be described in this way. An important question involved in this Taylor expansion is up to what degree it has to be extended to be sure that the principal non-linear hydrodynamic effects are described correctly. On the other hand it is questioned to what extend it is necessary to retain a great number of terms in such a model for a reasonable accurate description of manoeuvres, even if the separate hydrodynamic effects involved can be measured with forced model tests. In other words it is suggested that, on the ground that during an actual manoeuvre the ratios of the variables satisfy just one relation, it might be possible to describe the joint effect of a number of terms by one term only. In this way a much simpler mathematical model would arise, the coefficients of which had to be considered functions of the coefficients of the original model. Van Leeuwen (1970) described some simple non-linear models based on these grounds.

A disadvantage of such simplified mathematical models is that its coefficients cannot be determined by uncoupling the three motions which means that they can only be derived from free running tests, either full-scale or model tests. For practical purposes however, such as simulation studies and automatic piloting, these simplified non-linear models can be applied successfully.

The principle of the mathematical model used for the present model-tests is, apart

from some details, the same as has been used by Abkowitz. The way in which Abkowitz treats the influence of a change of the forward speed, however, brings about that no insight is gained into the physical background of this influence.
In this paper, the hypothesis is used that if the motions are similar, regarding velocities and accelerations, the principal hydrodynamic forces on the hull are proportional with the square of the instantaneous forward speed. For the forces, which mainly depend on the effective angle of attack of the rudder, proportionality with the square of the local water velocity is assumed.
The general concept of this hypothesis is confirmed by the model experiments. In the following chapter this will be discussed in more detail.

2 Equations of Motion

2.1 Introduction

If we form a mathematical model and we start from the fact that the hydrodynamic forces are functions of the velocities and accelerations involved in a motion, we can expand these forces, as has been done by Abkowitz (1964), in a Taylor series of these velocities and accelerations. On the ground of considerations of magnitude we can ignore the terms whose order is higher than e.g. the third. There are some objections to this procedure, however. Considering a term proportional to the third power of e.g. the angular velocity the omission of the fourth order terms means that the contribution of this term, regardless the forward speed, remains proportional with the third power of the angular velocity. From model experiments it is known that this - and similar terms - are reversed proportional with the forward speed. Neglecting this speed dependence consequently corresponds with underestimating the non-linear effects described by these third order terms in the case of speed reduction. For a speed reduction of 50 per cent, such a non-linear effect is underestimated by a factor two.
Another objection, though of less importance, is that if the separate velocities are considered as lateral, forward and angular velocity, the particular role played by the forward speed becomes hardly apparent.
In section 2.3, a different basis has been chosen for the mathematical model, the hypothesis mentioned in chapter 1 being used.
The effects of the fourth degree terms, mentioned above, are involved in the third degree Taylor expansion of the forces, if they are considered to be functions of characteristic variables, describing the similarity of the motions.
It is emphasised however, that the concept of this is not new, because also Davidson and Schiff (1946), Nomoto (1957) and Eda and Crane (1962) already paid attention to the importance of these variables. Both earlier work and the present investigation justify the adoption of the hypothesis concerning the forces.

2.2 Components of Hydrodynamic Forces

The equations of motion describing the balance of forces and moments during a still water manoeuvre can be written as follows (see also Figure 2):

$$m \cdot \left(\dot{v} + U_x r \right) = Y$$
$$I_{zz} \cdot \dot{r} = N$$
$$m \cdot \left(\dot{U}_x - vr \right) = X$$

Equation 1-a,b,c

where Y represents the component of the hydrodynamic forces perpendicular to the ship and N the corresponding moment, while X represents the component of

these forces acting in longitudinal direction.

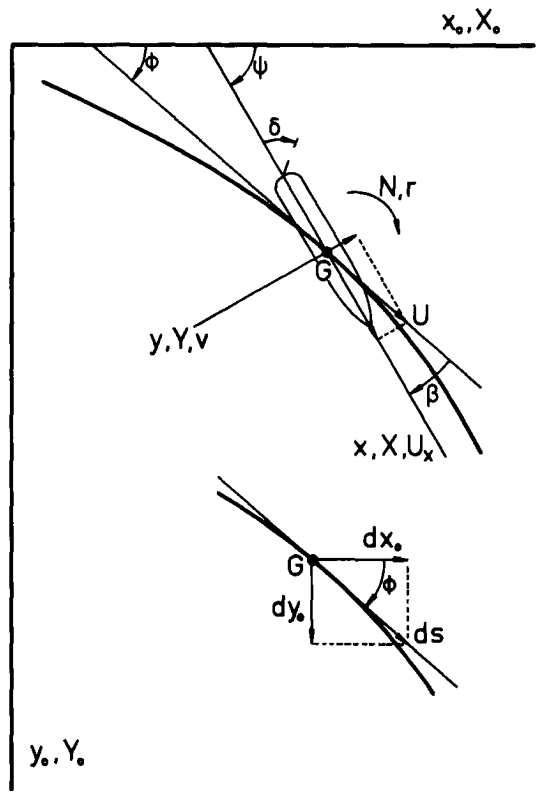

Figure 2 Co-ordinate System and Definition of Variables

The sum of the hydrodynamic forces can be divided into three groups:

1. The first group contains the components, which depend on the condition of motion of the ship without propeller and rudder. The variables involved in this case will be discussed in section 2.3.
2. The second group contains the forces, which act on the rudder. They depend on the effective angle of attack of the rudder and as this quantity depends on the ship's condition of motion, these components will depend on the variables of the first group as well as on the rudder angle itself.
3. The third group contains the force components, which are caused, among other things, by the change of circulation around the ship, due to the rudder deflection. In general, these components are considered to be the result of the fact that the sum of the hydrodynamic forces is not obtained by the superposition of the forces acting on the hull and those on the rudder, which may be approximately true for the side forces on sailing yachts.

Concerning the longitudinal force balance, a fourth group has to be considered, which involves the forces due to the resistance and the change of thrust caused by speed loss during manoeuvring. This group determines the difference between the forward speed of the centre of gravity and the speed of the water near the rudder.

2.3 Hypothesis Concerning the Hydrodynamic Forces Acting on the Manoeuvring Ship

The hypothesis mentioned in the preceding chapter, concerning the first group forces, is formulated as follows:

If two similar motions of a certain ship (or model) are compared, than these forces will be proportional to the square of the forward speeds involved, provided these speeds do not differ too much.

This hypothesis is mainly based on model experiments, though the results of full-scale manoeuvres, executed at different forward speeds, provide an indication for it as well.

The explanation for the usefulness of this hypothesis can be derived from the principal importance of the inertia forces and further from the small role played by the generated waves in a certain speed range.

If comparing the similar motions of a ship and her model, the wave patterns will only be similar if the Froude numbers in this case are equal, due to the constant value of the acceleration of gravity. On the ground of the small influence mentioned of the generated waves in a certain speed-range, the hypothesis is to be applied in this case within a restricted range of Froude

numbers, while the forces are proportional to the factor U^2L^2.
Concerning the forward speed, the upper limit of the usefulness of the hypothesis logically follows from the increasing importance of the waves, when the speed is higher.
The lower limit, however, cannot be derived only from the decreasing wave generation, as this, on the contrary, rather is a reason to expect its usefulness. Apparently there are other reasons for this, the principal of which probably is the increasing importance of the frictional forces, and in general, of the viscous effects, compared to the inertia forces.
The equations of motion of a floating body, moving in a horizontal plane, can be written in such a form, that the hypothesis is expressed by it. According to the hypothesis the forces, acting on the body, depend linearly on the force unit $0.5\rho U^2L^2$, so that the forces, divided by this unit, can only be functions of non-dimensional parameters, which describe the (restricted) similarity of the instantaneous conditions of motion to be compared.
Assuming only the velocities (v, r, U) and the accelerations ($\dot{v}$, $\dot{r}$, $\dot{U}$) to play a role in the equilibrium of forces, the equations of motion can be written as follows:

$$m\cdot\left(\dot{v}+U_x r\right)=\frac{1}{2}\rho U^2L^2\cdot \cdot Y^*\left(\frac{v}{U},\frac{L\cdot r}{U},\frac{L\cdot\dot{v}}{U^2},\frac{L^2\cdot\dot{r}}{U^2},\frac{L\cdot\dot{U}}{U^2}\right)$$

$$I_{zz}\cdot\dot{r}=\frac{1}{2}\rho U^2L^3\cdot \cdot N^*\left(\frac{v}{U},\frac{L\cdot r}{U},\frac{L\cdot\dot{v}}{U^2},\frac{L^2\cdot\dot{r}}{U^2},\frac{L\cdot\dot{U}}{U^2}\right)$$

$$m\cdot\left(\dot{U}_x-vr\right)=\frac{1}{2}\rho U^2L^2\cdot \cdot X^*\left(\frac{v}{U},\frac{L\cdot r}{U},\frac{L\cdot\dot{v}}{U^2},\frac{L^2\cdot\dot{r}}{U^2},\frac{L\cdot\dot{U}}{U^2}\right)$$

Equation 2-a,b,c

If the principle of the hypothesis is also applied to the force components of the second group, then the local similarity is characterised by the actual angle of attack of the rudder, while the forces are then proportional to the square of the local water velocity.
As the actual angle of attack and the magnitude and the direction of the local water velocity, these forces may be approximated as follows:

$$\overline{Y}=\frac{1}{2}\rho {U_R}^2L^2\cdot\overline{Y}\left(\delta_{act}\right)$$

where U_R is the local water velocity and

$$\delta_{act}=p_1\cdot\delta+p_2\cdot v^*+p_3\cdot r^*$$

with:

$$v^*=\frac{v}{U}\quad\text{and}\quad r^*=\frac{L\cdot r}{U}$$

Concerning the components of the third group, it is assumed that they will mainly depend on the variables of both the first and second group. They will partly be proportional to the square of the forward speed of the centre of gravity and for the rest to the square of the local (rudder) speed.
On this basis the mathematical model can be build up, considering the three groups to be functions of the non-dimensional variables, concerned. The expansion of the three groups in a third degree Taylor series leads to a number of terms a part of which being proportional with the square of the forward speed, while the remaining terms will be proportional to the square of the local rudder speed.

Considering e.g. the linear term in v^*, then the following expression is found:

$$\frac{1}{2}\cdot\rho L^2\cdot\left\{a_1 v^* U^2 \right.$$ (1st group: forces on hull without rudder and propeller)

$$+ a_2 v^* U_R{}^2$$ (2nd group: forces on rudder due to effective angle of attack)

$$\left. + \left(a_{31}U^2 + a_{32}U_R{}^2\right)v^*\right\}$$ (3rd group: interaction rudder-hull; forces due to failing of superposition principle)

The expressions for the other terms will have similar forms. On this ground the mathematical model is to be written in the following form:

$$m\cdot\left(\dot{v}+U_x r\right)=\frac{1}{2}\rho U^2 L^2 Y_1^* + \frac{1}{2}\rho U_R{}^2 L^2 \overline{Y}_2$$

$$I_{zz}\cdot\dot{r}=\frac{1}{2}\rho U^2 L^3 N_1^* + \frac{1}{2}\rho U_R{}^2 L^3 \overline{N}_2$$

$$m\cdot\left(\dot{U}_x - vr\right)=\frac{1}{2}\rho U^2 L^2 X_1^* + \frac{1}{2}\rho U_R{}^2 L^2 \overline{X}_2 + X_3$$

Equation 3-a,b,c

In these equations the components marked with an asterisk contain the terms originated from the Taylor expansions of the first and second group. The dashed components contain the corresponding terms of the second and third group. Both asterisk and dash marked components are functions of the rudder angle and the five variables determine the second order similarity. The longitudinal force component X_3 describes the difference between the ship's straight-line resistance and the change of thrust due to the speed reduction.

On the ground of theoretical considerations and the experience from earlier investigations a number of assumptions have been made, which simplify the expressions for the various components. Some of these assumptions have been investigated particularly, while others are not contradicted by the measurements.

The assumptions concerned are summarised as follows:

1. The forward speed U, as a variable of Equation 3, can be replaced by its longitudinal component U_x. Consequently, the variables v^* and r^* are defined as v/U_x and $L\cdot r/U_x$ respectively, while the unit ds^* is defined as $U_x\cdot dt/L$.
2. The hydrodynamic lateral forces are independent of the longitudinal acceleration, and the hydrodynamic longitudinal forces are independent of the sway and yaw accelerations.
3. Non-linear acceleration effects do not occur in the range of interest.
4. If the ship is on a straight course, the forces due to a certain rudder deflection are proportional to the square or the local rudder speed U_R. (This assumption may be considered the definition of the quantity U_R for the present investigations).
5. The influence of the rudder rate on added mass effects is negligible for practical purposes.

2.5 Set of Equations of Motion

Executing the Taylor expansions of the three groups of forces and moments and applying the assumptions indicated above, the equations of motion can be written as follows:

$$\left\{m' - \left(Y_{\dot{v}}^{*} + \overline{Y}_{\dot{v}} \frac{U_R'^2}{(1+u')^2}\right)\right\}\dot{v}' - \left\{Y_{\dot{r}}^{*} + \overline{Y}_{\dot{r}} \frac{U_R'^2}{(1+u')^2}\right\}\dot{r}' =$$
$$\left\{Y_v^{*}(1+u') + \overline{Y}_v \frac{U_R'^2}{1+u'}\right\}v' + \left\{(Y_r^{*} - m')(1+u') + \overline{Y}_r \frac{U_R'^2}{1+u'}\right\}r' +$$
$$\left\{Y_{vvv}^{*} \frac{1}{1+u'} + \overline{Y}_{vvv} \frac{U_R'^2}{(1+u')^3}\right\}v'^3 + \left\{Y_{rrr}^{*} \frac{1}{1+u'} + \overline{Y}_{rrr} \frac{U_R'^2}{(1+u')^3}\right\}r'^3 +$$
$$\left\{Y_{vrr}^{*} \frac{1}{1+u'} + \overline{Y}_{vrr} \frac{U_R'^2}{(1+u')^3}\right\}v'r'^2 + \left\{Y_{rvv}^{*} \frac{1}{1+u'} + \overline{Y}_{rvv} \frac{U_R'^2}{(1+u')^3}\right\}r'v'^2 +$$
$$\left\{Y_{\delta vv}^{*} + \overline{Y}_{\delta vv} \frac{U_R'^2}{(1+u')^2}\right\}\delta v'^2 + \left\{Y_{\delta rr}^{*} + \overline{Y}_{\delta rr} \frac{U_R'^2}{(1+u')^2}\right\}\delta r'^2 +$$
$$\left\{Y_{v\delta\delta}^{*}(1+u') + \overline{Y}_{v\delta\delta} \frac{U_R'^2}{1+u'}\right\}v'\delta^2 + \left\{Y_{r\delta\delta}^{*}(1+u') + \overline{Y}_{r\delta\delta} \frac{U_R'^2}{1+u'}\right\}r'\delta^2 +$$
$$\left\{Y_{vr\delta}^{*} + \overline{Y}_{vr\delta} \frac{U_R'^2}{(1+u')^2}\right\}v'r'\delta + \left\{Y_a^{*}(1+u')^2 + \overline{Y}_a U_R'^2\right\} +$$
$$\left\{\overline{Y}_\delta \delta + \overline{Y}_{\delta\delta\delta}\delta^3\right\}U_R'^2$$

Equation 4-a

$$\left\{I_{zz}' - \left(N_{\dot{r}}^{*} + \overline{N}_{\dot{r}} \frac{U_R'^2}{(1+u')^2}\right)\right\}\dot{r}' - \left\{N_{\dot{v}}^{*} + \overline{N}_{\dot{v}} \frac{U_R'^2}{(1+u')^2}\right\}\dot{v}' =$$
$$\left\{N_v^{*}(1+u') + \overline{N}_v \frac{U_R'^2}{1+u'}\right\}v' + \left\{N_r^{*}(1+u') + \overline{N}_r \frac{U_R'^2}{1+u'}\right\}r' +$$
$$\left\{N_{vvv}^{*} \frac{1}{1+u'} + \overline{N}_{vvv} \frac{U_R'^2}{(1+u')^3}\right\}v'^3 + \left\{N_{rrr}^{*} \frac{1}{1+u'} + \overline{N}_{rrr} \frac{U_R'^2}{(1+u')^3}\right\}r'^3 +$$
$$\left\{N_{vrr}^{*} \frac{1}{1+u'} + \overline{N}_{vrr} \frac{U_R'^2}{(1+u')^3}\right\}v'r'^2 + \left\{N_{rvv}^{*} \frac{1}{1+u'} + \overline{N}_{rvv} \frac{U_R'^2}{(1+u')^3}\right\}r'v'^2 +$$
$$\left\{N_{\delta vv}^{*} + \overline{N}_{\delta vv} \frac{U_R'^2}{(1+u')^2}\right\}\delta v'^2 + \left\{N_{\delta rr}^{*} + \overline{N}_{\delta rr} \frac{U_R'^2}{(1+u')^2}\right\}\delta r'^2 +$$
$$\left\{N_{v\delta\delta}^{*}(1+u') + \overline{N}_{v\delta\delta} \frac{U_R'^2}{1+u'}\right\}v'\delta^2 + \left\{N_{r\delta\delta}^{*}(1+u') + \overline{N}_{r\delta\delta} \frac{U_R'^2}{1+u'}\right\}r'\delta^2 +$$
$$\left\{N_{vr\delta}^{*} + \overline{N}_{vr\delta} \frac{U_R'^2}{(1+u')^2}\right\}v'r'\delta + \left\{N_a^{*}(1+u')^2 + \overline{N}_a U_R'^2\right\} +$$
$$\left\{\overline{N}_\delta \delta + \overline{N}_{\delta\delta\delta}\delta^3\right\}U_R'^2$$

Equation 4-b

$$\left\{m' - \left(X_{\dot{u}}{}^{*} + \overline{X}_{\dot{u}} \frac{U_R{}'^2}{(1+u')^2} \right)\right\}\dot{u}' =$$
$$\left\{X_{vv}{}^{*} + \overline{X}_{vv} \frac{U_R{}'^2}{(1+u')^2}\right\}v'^2 + \left\{X_{rr}{}^{*} + \overline{X}_{rr} \frac{U_R{}'^2}{(1+u')^2}\right\}r'^2 +$$
$$\left\{X_{vr}{}^{*} + m' + \overline{X}_{vr} \frac{U_R{}'^2}{(1+u')^2}\right\}v'r' + \left\{X_{r\delta}{}^{*}(1+u') + \overline{X}_{r\delta} \frac{U_R{}'^2}{1+u'}\right\}r'\delta +$$
$$\left\{X_{\delta v}{}^{*}(1+u') + \overline{X}_{\delta v} \frac{U_R{}'^2}{1+u'}\right\}\delta v' + \left\{\overline{X}_{\delta\delta} U_R{}'^2\right\}\delta^2 +$$
$$\left\{X_R{}^{*}(1+u')^2 - X_R{}^{*}\right\} + X_T{}'u'$$

Equation 4-c

In these equations all variables have been made non-dimensional with the initial speed U_0 so that e.g.:

$$u' = \frac{U_x}{U_0} - 1$$
$$v' = v^{*}(1+u')$$
$$r' = r^{*}(1+u')$$

Some additional remarks concerning these equations:

a. The side force and moment equations contain some terms to describe the asymmetrical behaviour of the ship. With zero rudder deflection these terms are $Y_a{}^{*}(1+u')^2 + \overline{Y}_a U_R{}'^2$ and $N_a{}^{*}(1+u')^2 + \overline{N}_a U_R{}'^2$ while the asymmetrical rudder effectiveness is described by the terms $\overline{Y}_{\delta\delta}\delta^2$ and $\overline{N}_{\delta\delta}\delta^2$ respectively.
b. The longitudinal force component X_3 is divided into two components, the first of that describes the balance between the original thrust and the straight-line resistance while the second describes the (linearised) increment of the thrust during a manoeuvre.
c. The fourth degree terms, which were mentioned in the introduction, are due to the factors $1/(1+u')$, which may be linearised in the range $-0.60 < u' < 0.00$ to $0.84 - 2.30 \cdot u'$.
d. If the change of speed during a manoeuvre is larger than the range in which the hypothesis is valid, than the star and dash coefficients can be considered linear functions of the speed. In that case additional coefficients as $Y_{vu}{}^{*}$ and $\overline{Y}_{vu}$ should be added. For the present investigation, this appeared not necessary however.

3 Execution of Tests

3.1 Measuring Equipment

The principal property of the measuring equipment is that only harmonic components of the forces are determined. For the present investigation only the first harmonic components were needed. This determination is achieved by multiplying the forces by $\sin\omega t$ and $\cos\omega t$ respectively, while these products are integrated during one or more periods of the oscillation. The non-oscillatory components of the forces are determined by integration of the force during a number of periods.

Zunderdorp and Buitenhek (1963) give in a more detailed discussion on the oscillator and the measuring equipment.
The static drift angle adjustment during the oscillation tests is achieved by turning the model with respect to the connecting line of the oscillator struts (the "pure yawing line"). This is sketched in Figure 3.

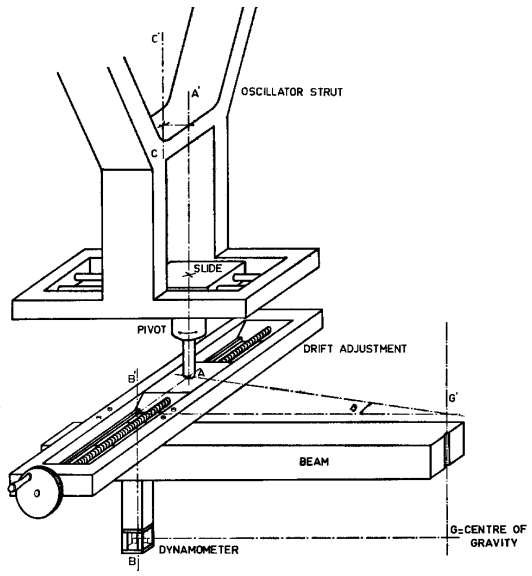

Figure 3 Drift Angle Adjustment of Oscillator

3.2 Determination of Draught and Trim

As the model was restrained from heaving and pitching the draught and trim, as dependent on the forward speed and the number of propeller revolutions had to be determined.
The revolutions adjusted for these tests were estimated from the available full-scale data. A change of the rpm did influence neither the mean draught nor the trim however. In Table 2 the various draughts fore and aft for model and ship are given.
These draughts have been adjusted for the tests concerned. It is questioned however if it is correct to restrain the model in vertical direction during oscillation and other tests.

model			ship		
U_0 (m/sec)	draught fore (mm)	draught aft (mm)	U_0 (kn)	draught fore (ft)	draught aft (ft)
1.080	236.0	229.3	15.5	42.6	41.4
.864	232.7	229.1	12.4	42.0	41.3
.648	230.3	229.0	9.3	41.5	41.3
.432	228.9	228.3	6.2	41.3	41.2
0	227.2	227.2	0	41.0	41.0

Table 2 Trim as Function of Speed

A particular investigation might give the answer, but it is not expected that undesirable cross-coupling effects would disturb the side force measurements, due to the uncoupling of the swaying and yawing motion. This is also expected with respect to the rolling motion. As it was not the purpose of this investigation to find an answer to this question, it was considered a useful approximation to adjust the constant draughts, derived from straight-line tests and to restrain the model also from rolling.

3.3 Determination of Resistance and Propulsion Coefficients

The description of the balance between longitudinal resistance and the propeller thrust is partly based on some full-scale of rpm at 15.5 knots and partly on the propeller characteristics. From these data the wake fraction was derived while for the lower speeds, caused by manoeuvring. This wake fraction was considered constant. From the fact that during a manoeuvre the power does not change, the increment of thrust and the decrement of rpm could be calculated using the propeller characteristics. For comparison purposes also the full-scale measurements of these quantities are given in Figure 4 and Figure 5.
Concerning the other initial speeds, 12.4, 9.3 and 6.2 knots, a linear relation between these speeds and the rpm was adopted (see Figure 6).
The increase of thrust and the decrease of the rpm during manoeuvres with these

initial speeds were determined as this was done for the 15.5 knots initial speed.

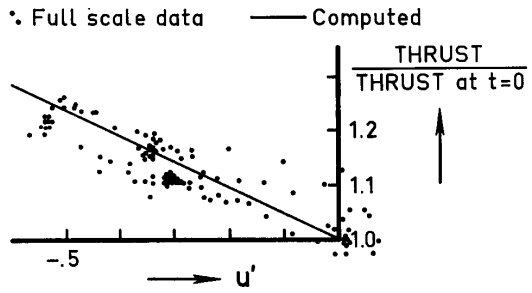

Figure 4 Variation of Thrust with Speed during Turning Circles at 100 Nominal RPM at t = 0

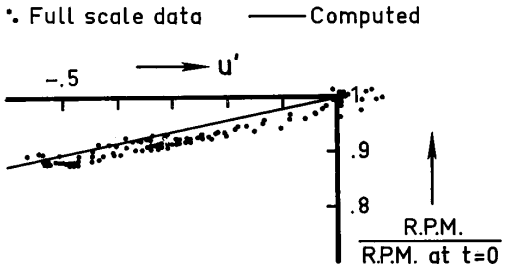

Figure 5 Variation of RPM with Speed during Turning Circles at 100 Nominal RPM at t = 0

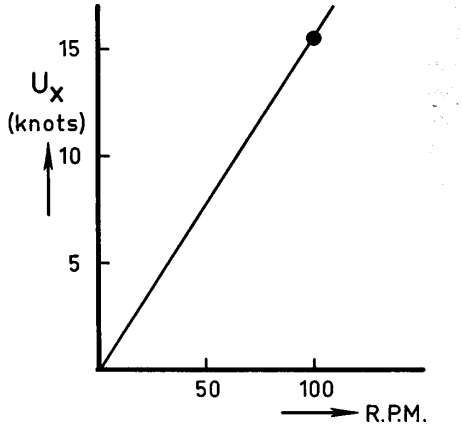

Figure 6 Adopted Initial Speed-RPM Relation

In Figure 7 and Figure 8 the calculated thrust and torque are plotted for the initial conditions.

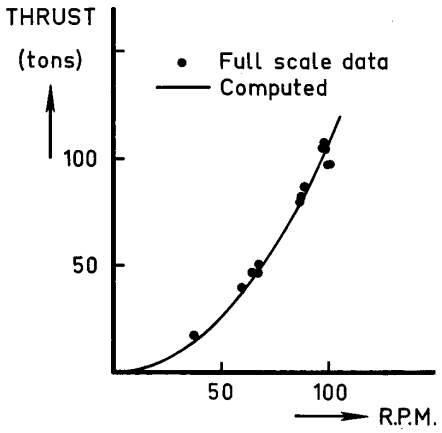

Figure 7 Measured and Computed Values of Thrust

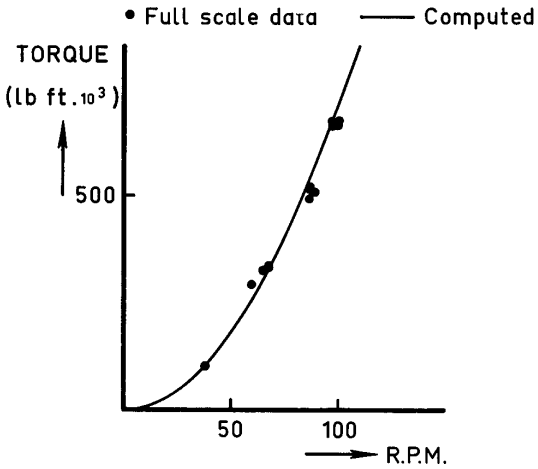

Figure 8 Measured and Computed Values of Torque

It can be shown that on a straight course a parabolic relation between the thrust and the forward speed exists, provided the thrust curve of the propeller diagram is linearised in the range of interest. Consequently the assumption of a parabolic relation between the longitudinal resistance and the speed is equivalent to the assumption of a speed-independent thrust deduction fraction. This number was estimated to be 0.20.

On this basis the resistance coefficient X_R^* was calculated:

$$X_R^* = -54.0 \cdot 10^{-5}$$

while for the effective thrust increment coefficient X_T' was found:

$$X_T' = -25.0 \cdot 10^{-5}$$

In Table 3 the computed rps, concerning the various conditions, are summarised.

$U_0 = 1.080$ m/sec			$U_0 = .864$ m/sec			$U_0 = .648$ m/sec			$U_0 = .432$ m/sec		
U_x	u'	rps	U_x	u'	rps	U_x	u'	rps	U_x	u'	rps
1.080	0	12.85									
.864	−.20	12.30	.864	0	10.23						
.648	−.40	11.80	.648	−.25	9.70	.648	0	7.73			
.432	−.60	11.33	.432	−.50	9.21	.432	−.33	7.20	.432	0	5.12

Table 3 Computed Propeller Rate Values

It is noted however that these data are corrected for the differences between the full-scale and model propeller (U 218 - B 5.60 respectively).
The rps values, adjusted during the model tests, are not the same as given in Table 3, however, as originally these values were based on the full-scale relation between thrust and speed as given by Clarke (1965). During the analysis of the test data this relation did not appear to correspond with the full-scale data of rpm and the propeller diagram, consequently nor did the rpm-*U* relation. This is shown in Figure 9.

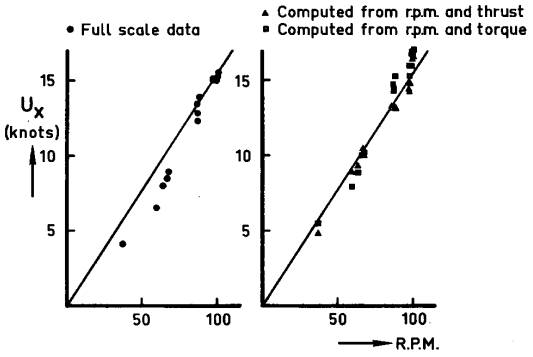

Figure 9 Discrepancies between the Measured Forward Speed and the Speed Derived from Thrust and Torque Measurements (Full-Scale)

From this figure it is assumed that the full-scale speed measurements concerned are not correct.

As, in addition, the coefficients, which describe the balance between resistance and thrust during a manoeuvre based on this relation, resulted in very large differences between the manoeuvres computed and those executed on full-scale, the linear relation between rpm and speed was adopted.
The coefficients of the force and moment components $\overline{Y}_2$, $\overline{N}_2$ and $\overline{X}_2$ have been corrected as far as necessary, which was possible because their relation with the rpm was known from the model experiments.

3.4 Determination of Rudder Speed U_R

The quantity U_R has been derived from the straight-line tests with constant rudder angle. These tests were executed for the 10 combinations of speed and rps, while in each case the rudder angle was varied from 36 degrees port to 36 degrees starboard with steps of 9 degrees. A formal description of the water velocity near the rudder has been based on the impulse theory with respect to the propeller. According to this theory the water velocity at a certain distance from the propeller disk can be written as (see Figure 10):

$$U_R' = V_e' + \mu \cdot C_a'$$

Equation 5

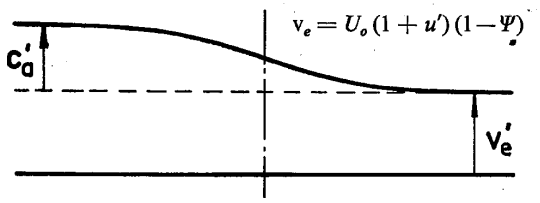

Figure 10 Change of Water Velocity near the Propeller

In both cases the prime denotes making it non-dimensional with the initial speed U_0. If the curves of the propeller torque and thrust are linearised in the speed range of interest the expression for C_a' can be written as follows:

$$\left(\frac{C_a'}{V_e'}+1\right)^2 = 1+\frac{a_2}{\Lambda}+\frac{a_1}{\Lambda^2}$$

Equation 6

where the coefficients a_1 and a_2 describe the linearised torque and thrust.

Using the wake fraction ψ (see chapter 3.2), the values of C_a' can be calculated for each of the 10 speed-rps combinations given in . If these values are applied to Equation 6, the unknown speed U_R' is replaced by the quantity μ, which originally indicated the distance from the propeller disk. It must be noted however that in this case the deviations due to the assumptions used culminate at the computation of μ, so that this quantity rather has to be considered a calculation quantity than an indication for the distance between rudder and propeller. The same is to be applied to the quantity U_R'.

Substitution of the expression for U_R' into the formal description of the side force and moment measurements at $v^* = r^* = 0$, for each of the rudder angles applied, a value of μ was obtained. In Figure 11 the products $\mu \cdot \delta$ has been plotted versus the rudder angle from which the optimal value of 0.376 was derived.

Using this value of μ, the values of $U_R'^2$ were calculated and plotted in Figure 12 versus the relative speed loss u'.

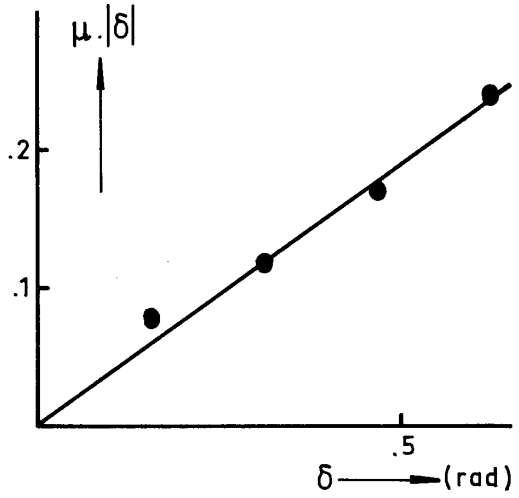

Figure 11 Experimental Determination of Factor μ from Equation 5

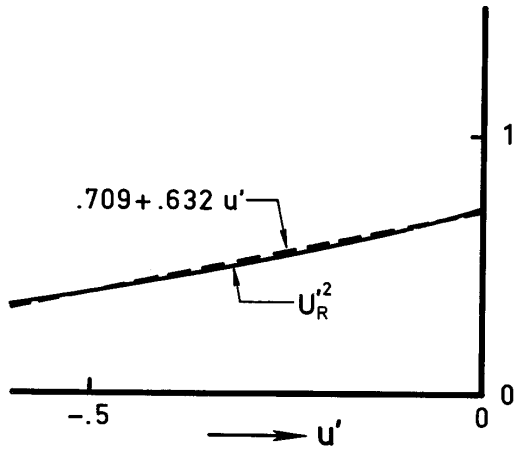

Figure 12 Linearisation of the Quantity $U_R'^2$

In Figure A 1 (Appendix A), for the 10 combinations of speed and rpm the measured rudder forces and moments are plotted on the basis of $U_R'^2$ while the rudder angle is a parameter.

The values of Y_a and N_a were too small to distinguish between star and dash components. A mean value, derived from the swaying tests and the present tests is obtained.

actual speed		1.08 m/sec	.86 m/sec		.65 m/sec			.43 m/sec			
r.p.s.		12.38	11.95	10.29	11.54	9.85	8.34	11.20	9.53	8.00	6.50
β	$\lvert v^* \rvert$										
±4°	.0698	θ	θ	θ	θ	θ	θ	θ	θ	θ	θ
±8°	.1392	θ	θ	θ	θ	θ	θ	θ	θ	θ	θ
±12°	.2079	θ	θ	θ	θ	θ	θ	θ	θ	θ	θ
±13.8°	.2385		θ	θ	θ	θ	θ	θ	θ	θ	θ
combined drift and rudder tests	$\lvert\delta\rvert$	9 18 27 36	9 18 27 36	9 18 27 36	9 18 27 36	9 18 27 36	9 18 27 36	9 18 27 36	9 18 27 36	9 18 27 36	9 18 27 3
	+	θ θ θ θ	θ θ θ θ θ θ θ		θ θ θ θ	θ θ θ		θ θ θ θ			
	−	θ θ θ θ	θ θ θ θ		θ θ θ θ			θ θ θ θ			
$\beta=0$	+	θ θ θ θ	θ θ θ θ θ θ θ θ		θ θ θ θ	θ θ θ θ θ θ θ		θ θ θ θ θ θ θ θ θ θ θ θ			
	−	θ θ θ θ	θ θ θ θ θ θ θ θ		θ θ θ θ	θ θ θ θ θ θ θ		θ θ θ θ θ θ θ θ θ θ θ θ			

θ indicates that test was carried out.

Table 4 Static Sway Test Program

For the computation of the rudder coefficients the measurements concerned were corrected with these mean values.

3.5 Determination of Remaining Coefficients

3.5.1 Static Sway Tests

These tests, executed at the 10 combinations of speed and rpm, provided the coefficients of the following variables:

Y and N equation: v^*, v^{*3}, $v^*\delta^2$, $v^{*2}\delta$

X equation: v^{*2}, $v^*\delta$

while also the Y_a and N_a coefficients were determined.

In Table 4 a scheme of the test program concerned is given.

Using the test results at $\delta = 0$ the coefficients of v^*, v^{*3} and v^{*2} are determined while computing the $v^*\delta^2$, δv^{*2} and $v^*\delta$ coefficients; the coefficients first mentioned were considered to be known quantities.

In Figure A 2, Figure A 3 and Figure A 4, the side force and moment measurements concerned are plotted, while the longitudinal force measurements are shown in Figure A 12, Figure A 13 and Figure A 14.

As no information was available involving the influence of the rudder speed U_R, the dash coefficients concerned could not be determined.

3.5.2 Oscillatory Swaying Tests

These tests were mainly executed to determine the lateral added mass effect. Only two initial speed conditions are considered while the influence of a change of rpm appeared negligible. Consequently $\overline{Y}_{\dot{v}}$ and $\overline{N}_{\dot{v}}$ are set to zero. The range in which the non-dimensional acceleration $L \cdot \dot{v} / U_x^2$ was changed; it was extended to 0.25 though an estimation of the maximum full-scale value is about 0.15. Nevertheless the measured force appeared linear with the acceleration in the whole range.

In Figure A 5 the data concerned are plotted where the speeds are considered parameter.

3.5.3 Oscillatory Yawing Tests with Constant Drift and Rudder Angle

In general these tests were also executed for the ten conditions given in Table 3. The amplitude of the characteristic variable r^* was varied between 0.05 and 0.70 corresponding with turning radii of approximately 20 and 3 ship lengths respectively.

The choice of the oscillator frequency has been based on the following considerations:

a. Based on the tank width available and the properties of the oscillator the non-dimensional frequency $\gamma = \omega \cdot U_x / g$, which is the leading factor determining the oscillatory part of the wave pattern, was kept as small as possible. Concerning the influence of this variable the reader is referred to Van Leeuwen (1964).

b. The forces involved in the lowest speed, corresponding with a Froude number 0.07, had to be reasonably measurable.

In order to judge the frequency range used at these oscillatory motions, the quantity $2\pi / \omega^*$ can be used, indicating the number of ship lengths sailed during one period.
The restricted tank width and oscillator amplitude involves a disagreement between the forced motions of the model and full-scale manoeuvres e.g. sinus-response tests. These full-scale manoeuvres involve rather large amplitudes in the range of practical full-scale frequencies. It is not known, however, how far this discrepancy between model-scale and full-scale manoeuvres influences the hydrodynamic derivatives. In the references Van Leeuwen (1969a) and Van Leeuwen (1969b) some more details concerning this matter are discussed.

In Table 5 a scheme of the complete yawing program is given.

actual speed		1.08 m/sec	.86 m/sec		.65 m/sec			.43 m/sec			
r.p.s.		12.38	11.95	10.29	11.54	9.85	8.34	11.20	9.53	8.00	6.50
r_0^*	$2\pi/\omega^*$	γ	γ		γ			γ			
.05	5.03	.037									
.10	3.53	.053									
.15	2.87	.065			.019	.019	.019				
.20	2.47	.075	.048	.048	.027	.027	.027	.012	.012	.012	.012
.25	2.20							.013	.013	.013	.013
.30	1.99		.060	.060	.033	.033	.033	.015	.015	.015	.015
.35	1.83							.016	.016	.016	.016
.40	1.70		.070	.070	.039	.039	.039	.017	.017	.017	.017
.50	1.51		.079	0.79	.044	.044	.044				
.60	1.36		.087	.087	.049	.049	.049 [1]				
.70	1.24		.096	.096	.054	.054	.054 [1]				
driftangle (degree)		0 4 8 12	0 4 8 12	0 4 8 12	0 4 8 12	0 4 8 12	0 4 8 12	0 4 8 12	0 4 8 12	0 4 8 12	0 4 8 12
rudder-angle (degree)	0	θ θ θ θ	θ	θ θ θ θ	θ	θ	θ θ θ θ	θ	θ	θ	θ
	12	θ	θ	θ	θ	θ	θ	θ	θ	θ	θ
	18										
	24	θ	θ	θ	θ	θ	θ	θ	θ	θ	θ
	36	θ	θ	θ θ θ θ	θ	θ	θ θ θ θ	θ	θ	θ	θ

θ indicates that test was carried out.
[1]) test only carried out at $\delta = \beta = 0$.

$$r^* = \frac{L}{U_x} \cdot r \qquad \omega^* = \frac{L}{U_x} \cdot \omega \qquad \gamma = \frac{\omega \cdot U_x}{g}$$

$2\pi/\omega^*$ = number of shiplengths sailed during one period of oscillation.
Oscillator amplitude during these tests was .10 m.

Table 5 Yaw Test Program

The measured forces and moments concerning these tests are to be divided into three components:

a. proportional to the angular velocity (sine component)
b. proportional to the angular acceleration (cosine component)
c. the constant component.

In Table 6 the various components are summarised while the variables concerned are mentioned in the sequence of determination.

sine comp.		cosine comp.	constant comp.		variables varied
Y, N	X	Y, N	Y, N	X	
r^*, r^{*3}		$L^2\dot{r}/U_x^2$		r^{*2}	r^*
r^*v^{*2}	r^*v^*		v^*r^{*2}		r^*, v^*
$r^*\delta^2$	$r^*\delta$		δr^{*2}		r^*, δ
$r^*v^*\delta$					r^*, v^*, δ

Table 6 Variables and Components

Due to the criteria given in the preceding chapter, concerning the ranges of oscillator frequencies and amplitudes, the maximum value of the angular acceleration amplitude exceeds the corresponding value ever occurring at the full-scale ship, the latter being estimated about 1.30.

Consequently the coefficients concerned have been determined in this full-scale range the more so as outside this range the model experiments showed a considerable non-linear effect.

In Figure A 6 through Figure A 11 the side force and moment measurements are plotted, while in Figure A 14, Figure A 16 and Figure A 17 the corresponding longitudinal force measurements are given.

3.6 Some Experiments with a Small Model (α = 100)

For comparison purpose the results of a restricted number of tests with a small model are given. These tests have been executed before those with the larger model. Because of the very low speeds involved the results are considered not very trustworthy.

The test program consisted of:

a. static sway tests
b. oscillatory swaying tests
c. oscillatory yawing tests (without rudder angle and drift angle)

The influence of the speed reduction and consequently of the thrust increment was not examined in particular. It was assumed that the hypothesis mentioned in Chapter 2.4 would hold. This means that the tests only had to be executed for the initial speed conditions.

In Table 7 the results of these tests are summarised and are compared with those of the large model. In Figure A 18 through Figure A 27 the measurements are shown.

important coefficients				less important coefficients			
coeff.	1:55 model	1:100 model	diff. %	coeff.	1:55 model	1:100 model	diff. %
Y'_v	−1797	−1634	9	Y'_{vvv}	−8867	−11977	35
$Y'_r - m'$	− 774	− 863	12	Y'_{rrr}	+ 404	+ 303	25
Y'_δ	+ 330	+ 294	11	$Y'_{\delta\delta\delta}$	− 47	− 40	16
N'_v	− 473	− 473	0	N'_{vvv}	− 620	+ 360	150
N'_r	− 252	− 200	21	N'_{rrr}	− 270	− 323	20
N'_δ	− 164	− 132	19	$N'_{\delta\delta\delta}$	+ 27	+ 23	16
$m' - Y'_{\dot{v}}$	+2277	+2303	1	$N'_{\dot{v}}$	− 40	− 27	33
$I'_{zz} - N'_{\dot{r}}$	+ 128	+ 117	8	$Y'_{\dot{r}}$	− 65	− 28	57

Table 7 Coefficients of Small Model (1:100)

As follows from Table 7 for the important coefficients, the magnitude of the differences between the coefficients of the large and the small model is about 10 percent while this percentage for the less important coefficients is about 25.

$\delta_0 = -19°$

scale	1:100	1:55	full scale
advance (m)	993	985	972
transfer (m)	665	687	660
tactical diameter (m)	1255	1276	1233
diameter (m)	1086	1071	1100
r_c (degree/sec)	.453	.466	.490
U_{xc} (kn.)	8.48	8.59	9.10
β_c (degree)	10.5	9.9	9.5

Table 8 Comparison of 19^0 Starboard Circle for Scale 1:100, 1:55 and 1:1

The importance of these differences is partly shown in Table 8 in which the results of a turning circle manoeuvre are given, computed with the 1:100 model coefficients, completed with some of the large model.

Concerning the range of variables applied with this model it is noted that nearly the same maximum values of rudder angle, drift angle and angular velocity were adjusted. The difference between the frequency ranges of the two models is expressed by the two quantities $2\pi/\omega^*$, denoting the number of ship lengths covered during one period of the oscillation, and γ which quantity governs the wave pattern during the oscillatory motion.

The first quantity varies from 3.0 at $r_0^* = 0.10$ to 1.1 at $r_0^* = 0.50$, which is nearly the same range as is applied for the large model. The maximum value of γ at $r_0^* = 0.50$ (0.17) is about two times the corresponding value of the large model however. Nevertheless this value is considered sufficiently low as to avoid disturbing influences of this parameter.

Putting the results of the two models in the light of the hypothesis, mentioned in chapter 2.4, it appears that the hypothesis holds for both models separately, but not if comparing both models. As in both cases the Froude numbers had the same values the differences between the corresponding coefficients can be traced to the small Reynolds number of the small model.

3.7 Some Remarks Concerning Computed Coefficients

It is found that the rpm effect on the linear terms is very small, compared to the magnitude of these terms. Concerning the non-linear terms, it was not possible to distinguish between the normal scatter of the data and this rpm effect, due to the restricted accuracy of the measurements and the relatively small values of this non-linear term. This does not apply to the pure rudder angle dependant terms of course, the change of which with rpm is considerable.

Another important result is the usefulness of the hypothesis, concerning the proportionality of the forces with the square of the instantaneous speed and the characteristic variables v^* and r^*. This is clearly shown e.g. in Figure A 2, Figure A 3 and Figure A 6. Though it has also been tried to distinguish between the results concerning the four initial speeds by Van Leeuwen (1969c), it follows from the figures just mentioned that the differences, which could be considered a Froude number effect, are not significant however.

"asterisk"-model eq. (3a)			"Prime"-model eq. (4a)			
var.*	$C^*_{var.}$	$\overline{C}_{var.}$	var.′	$C'_{var.}$	var.′u′	$C'_{var.u}$
v^*	−1797	0	v'	−1797	$v'u'$	− 1797
r^* [1]	− 774	0	r' [1]	− 774	$r'u'$	− 774
δ	0	+330	δ	+ 234	$\delta u'$	+ 208
v^{*3}	−8867	0	v'^3	−7423	v'^3u'	+20394
r^{*3}	+ 404	0	r'^3	+ 339	r'^3u'	− 930
δ^3	0	− 47	δ^3	− 34	δ^3u'	− 30
v^*r^{*2}	−2208	0	$v'r'^2$	−1848	$v'r'^2u'$	+ 5078
$v^*\delta^2$	+ 277	0	$v'\delta^2$	+ 277	$v'\delta^2u'$	+ 277
r^*v^{*2}	+2562	0	$r'v'^2$	+2145	$r'v'^2u'$	− 5893
$r^*\delta^2$	0	0	$r'\delta^2$	0	$r'\delta^2u'$	0
δv^{*2}	+ 652	0	$\delta v'^2$	+ 652	$\delta v'^2u'$	0
δr^{*2}	+ 218	0	$\delta r'^2$	+ 218	$\delta r'^2u'$	0
$v^*r^*\delta$	+ 412	0	$v'r'\delta$	+ 412	$v'r'\delta u'$	0
δ^2	0	+ 40	δ^2	+ 28	δ^2u'	+ 25
1	− 14	0	1	− 13	u'	− 20
$L\dot{v}/U_x^2$ [1]	−2278	0	$\dot{v}'$ [1]	−2278	$\dot{v}'u'$	0
$L^2\dot{r}/U_x^2$	− 65	0	$\dot{r}'$	− 65	$\dot{r}'u'$	0

[1] These coefficients include the ship's mass m'.

Table 9 Lateral Force Coefficients

"asterisk"-model eq. (3b)			"Prime"-model eq. (4b)			
var.*	$C^*_{var.}$	$\overline{C}_{var.}$	var.′	$C'_{var.}$	var.′u′	$C'_{var.u}$
v^*	− 473	0	v'	− 473	$v'u'$	− 473
r^*	− 252	0	r'	− 252	$r'u'$	− 252
δ	0	−164	δ	− 116	$\delta u'$	− 103
v^{*3}	− 620	0	v'^3	− 519	v'^3u'	+1425
r^{*3}	− 270	0	r'^3	− 226	r'^3u'	+ 620
δ^3	0	+ 27	δ^3	+ 19	δ^3u'	+ 17
v^*r^{*2}	+ 395	0	$v'r'^2$	+ 331	$v'r'^2u'$	− 908
$v^*\delta^2$	− 69	0	$v'\delta^2$	− 69	$v'\delta^2u'$	− 69
r^*v^{*2}	−2191	0	$r'v'^2$	−1834	$r'v'^2u'$	+5040
$r^*\delta^2$	0	0	$r'\delta^2$	0	$r'\delta^2u'$	0
δv^{*2}	− 235	0	$\delta v'^2$	− 235	$\delta'v'^2u'$	0
δr^{*2}	− 104	0	$\delta r'^2$	− 104	$\delta r'^2u'$	0
$v^*r^*\delta$	− 232	0	$v'r'\delta$	− 232	$v'r'\delta u'$	0
δ^2	0	− 12	δ^2	− 8	δ^2u'	− 7
1	0	0	1	0	u'	0
$L\dot{v}/U_x^2$	− 40	0	$\dot{v}'$	− 40	$\dot{v}'u'$	0
$L^2\dot{r}/U_x^2$ [1]	− 128	0	$\dot{r}'$ [1]	− 128	$\dot{r}'u'$	0

[1] These coefficients include ship's moment of inertia I'_{zz}.

Table 10 Yaw Moment Coefficients

"asterisk"-model (eq. 3c)			"prime"-model (eq. 4c)			
var*	C^*_{var}	$\overline{C}_{var}$	var′	C'_{var}	var′u′	$C'_{var.u}$
v^{*2}	+ 88	0	v'^2	+ 88	v'^2u'	0
r^{*2}	0	0	r'^2	0	r'^2u'	0
δ^2	0	−177	δ^2	− 125	δ^2u'	−112
v^*r^* [1])	+2149	0	$v'r'$ [1])	+2149	$v'r'u'$	0
$r^*\delta$	− 50	0	$r'\delta$	− 50	$r'\delta u'$	− 50
δv^*	+ 117	0	$\delta v'$	+ 117	$\delta v'u'$	+117
$L\dot{u}/U_x^2$ [1])	−1329	0	$\dot{u}'$ [1])	−1329	$\dot{u}'u'$	0
resistance- and thrust coefficients						
X_R^*	− 54		u'	− 133	$u'u'$	− 54
X_T'	− 25					

[1]) These coefficients include the ship's mass m'.

Table 11 Longitudinal Force Coefficients

In Table 9, Table 10 and Table 11 in the left columns the coefficients of the set of Equation 3 are given while in the right columns the corresponding coefficients of Equation 4 are summarised, the latter being derived from the preceding ones. This derivation is partly based on the following approximations:

$$(1+u')^2 = 0.940 + 1.400 \cdot u'$$

$$\frac{1}{1+u'} = 0.837 - 2.300 \cdot u'$$

$$U_R'^2 = 0.709 + 0.632 \cdot u'$$

The accuracy of these approximations is shown in Figure 12, Figure 13 and Figure 14 in which these quantities are plotted. Concerning the signs of the coefficients in these tables the rule holds that all terms are transported to the right hand sides of the equations.

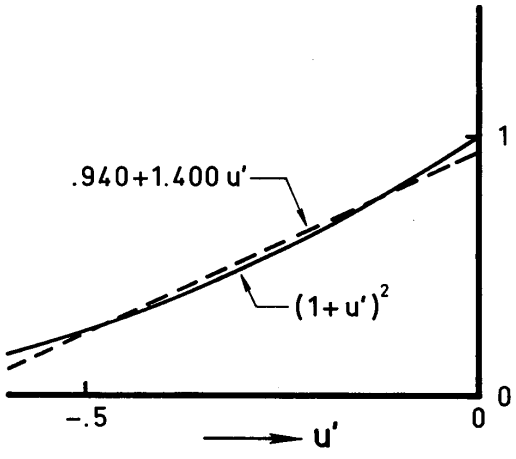

Figure 13 Linearisation of Speed Dependent Factor $(1+u')^2$

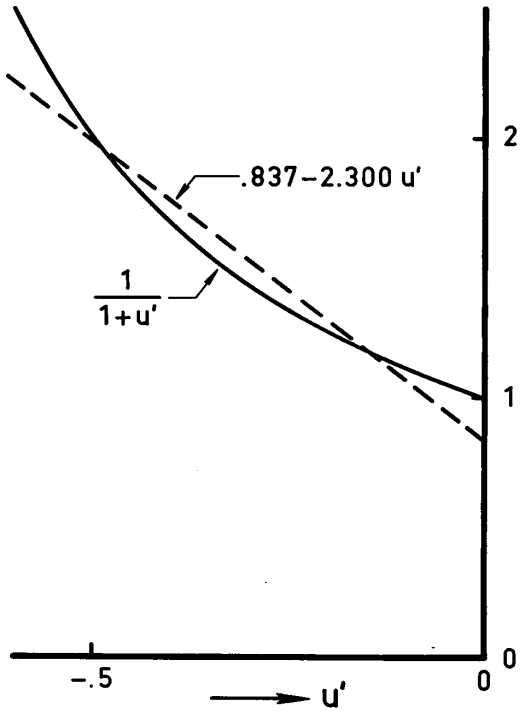

Figure 14 Linearisation of Speed Dependent Factor $1/(1+u')$

4 Computer Programs

4.1 Least Squares Analysis of Measured Data

This IBM 360/65 computer program SBSL#M03 has been developed to compute the coefficients of a fourth order polynomial of four variables:

$$F(x_1, x_2, x_3, x_4) = \sum_{t=1}^{p} C_t \cdot x_1^{\,k} x_2^{\,l} x_3^{\,m} x_4^{\,n}$$

using the least square criterion. Herein is $p \le 70$ and $k+l+m+n \le 4$.

If some of the coefficients are already known they can be given and the corresponding terms are subtracted from the measured value of the function. If the distance between a measurement and the computed value of the polynomial exceeds two times the RMS value the data concerned are dropped while the coefficients are computed again. This "data point selection procedure" primarily

serves to locate measuring, writing or typing errors. The factor 2 used in this criterion has been found experimentally. In statistics, usually a factor 3 is applied, though it has been found that if the number of measurement is relatively small even large errors are not located in that case.
This data point selection procedure comes into operation again, unless:

a. the number of selected data exceeds ten percent of the total number,
b. the RMS value is already smaller than a boundary value given beforehand.

In the next stage the maximum value of each term is computed. If these maximum contributions of a number of terms is smaller than the boundary value just mentioned the procedure is repeated, though without the coefficient the maximum contribution of which was the smallest.
Also this "coefficients selection procedure" is repeated until the contributions of all terms remained are sufficient.
Further the standard deviation and the correlation coefficient of each coefficient are computed. The first quantity is plotted in Figure 15 and Figure 16 concerning the large and the small model respectively.

A later PC version of this computer program can be found at the Internet: http://www.shipmotions.nl.

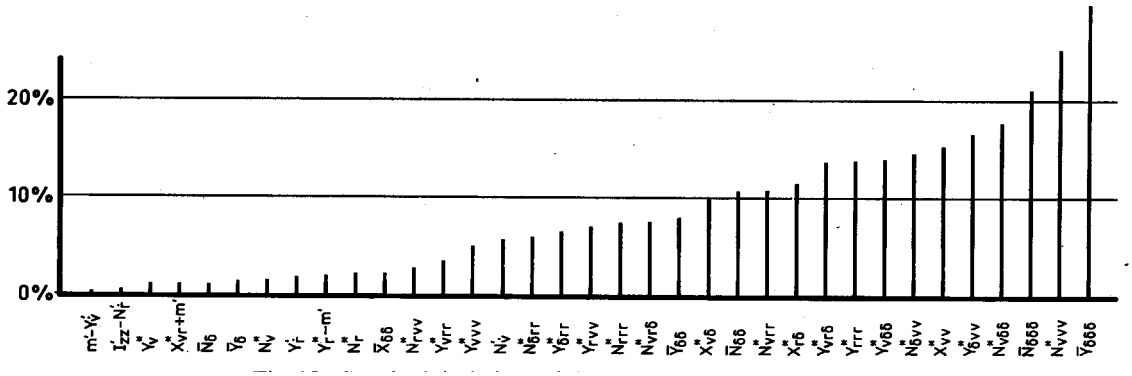

Figure 15 Standard Deviations of Coefficients

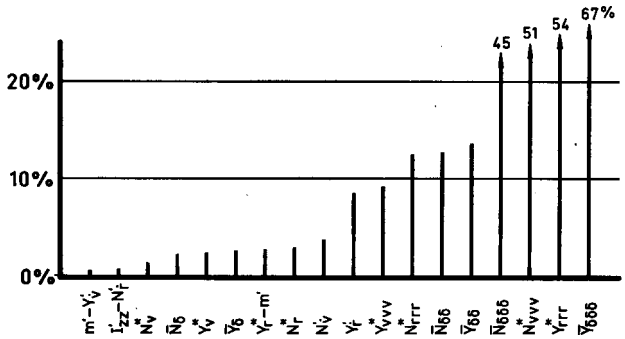

Figure 16 Standard Deviation of Coefficients (Small Model 1:100)

4.2 Solution of Differential Equations

In this computer program (IBM 360/65 program SBSL#M02) the differential equations are solved for given time depending rudder signals, where the Runge-Kutta procedure is applied. Two cases are considered. In the first the rudder rate is constant or zero, while in the second a sinusoidal rudder input can be given to determine the frequency characteristics of a ship.

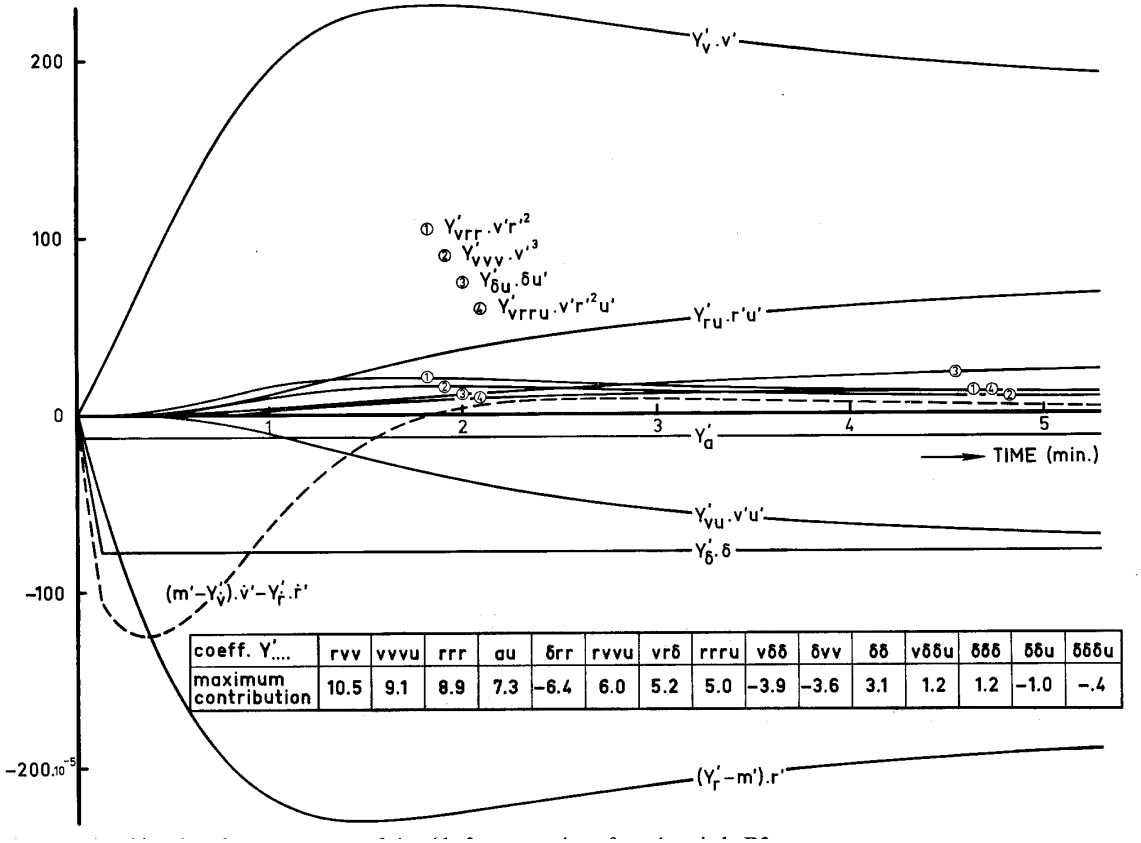

coeff. Y'....	rvv	vvvu	rrr	au	δrr	rvvu	vrδ	rrru	vδδ	δvv	δδ	vδδu	δδδ	δδu	δδδu
maximum contribution	10.5	9.1	8.9	7.3	−6.4	6.0	5.2	5.0	−3.9	−3.6	3.1	1.2	1.2	−1.0	−.4

Figure 17 Time Histories of Separate Terms of Side Force Equation of Turning Circle D2

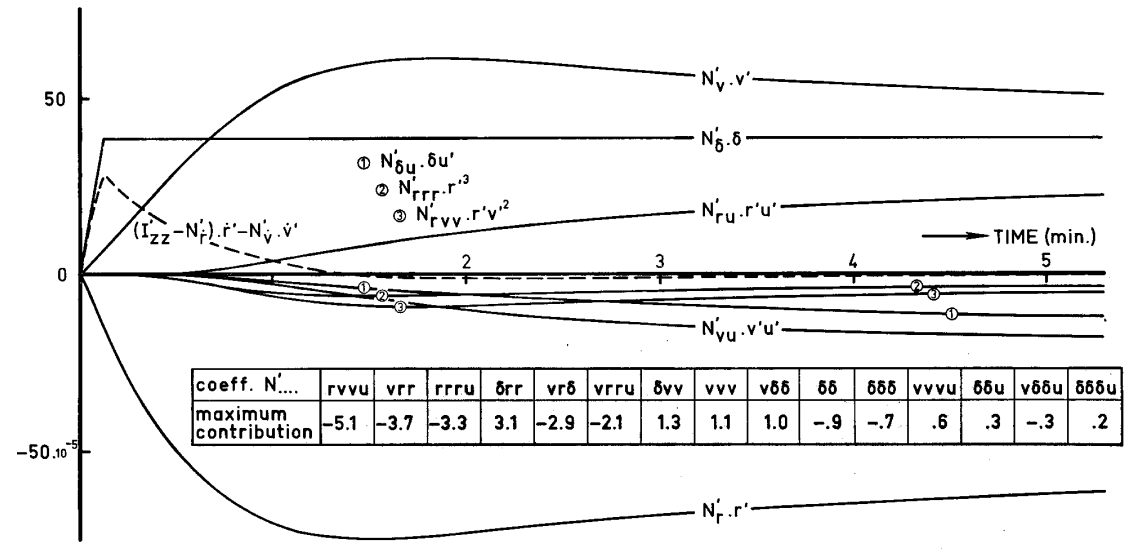

coeff. N'....	rvvu	vrr	rrru	δrr	vrδ	vrru	δvv	vvv	vδδ	δδ	δδδ	vvvu	δδu	vδδu	δδδu
maximum contribution	−5.1	−3.7	−3.3	3.1	−2.9	−2.1	1.3	1.1	1.0	−.9	−.7	.6	.3	−.3	.2

Figure 18 Time Histories of Separate Terms of Moment Equation of Turning Circle D2

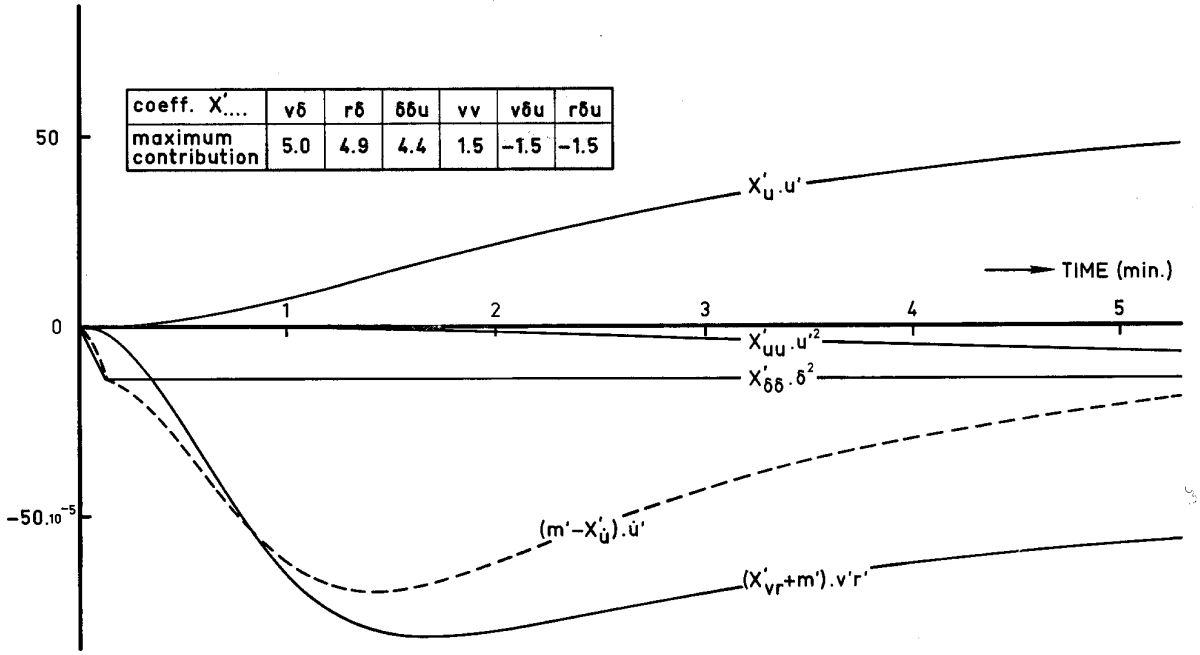

Figure 19 Time Histories of Separate Terms of Longitudinal Force Equation of Turning Circle D2

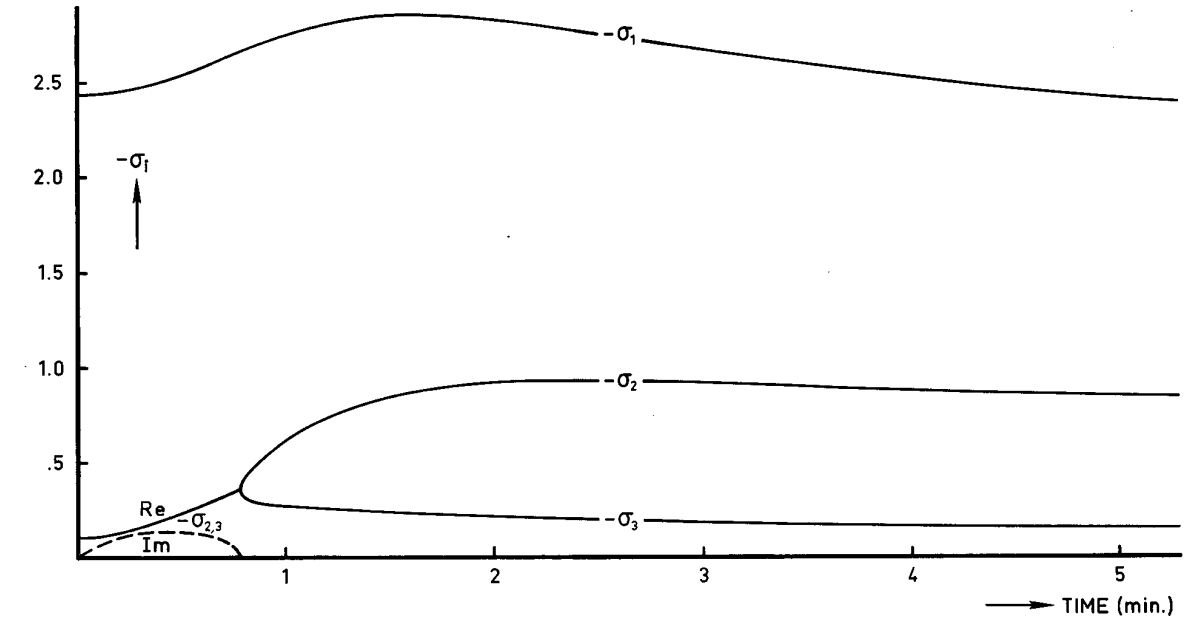

Figure 20 Time Histories of Stability Roots of Turning Circle D2

The output quantities can also be required to obtain the input for the coefficients program M03, to determine the coefficients of a mathematical model with a reduced number of coefficients. Further for each step the value of each term of the set of equations of motion is computed which enables to get an insight in the importance of the various components. An illustration of this is given in Figure 17, Figure 18 and Figure 19.

Another way to observe the process of a manoeuvre is to linearise the equations of motion at each step to the set:

$$\Delta\dot{v} = a_{11} \cdot \Delta v + a_{12} \cdot \Delta r + a_{13} \cdot \Delta\delta + a_{14} \cdot \Delta u$$
$$\Delta\dot{r} = a_{21} \cdot \Delta v + a_{22} \cdot \Delta r + a_{23} \cdot \Delta\delta + a_{24} \cdot \Delta u$$
$$\Delta\dot{u} = a_{31} \cdot \Delta v + a_{32} \cdot \Delta r + a_{33} \cdot \Delta\delta + a_{34} \cdot \Delta u$$

Using the coefficients of this set of equations the stability of the system can be observed. The time constants of the system can be found from the roots of the set:

$$\begin{vmatrix} a_{11}-\lambda & a_{12} & a_{14} \\ a_{21} & a_{22}-\lambda & a_{24} \\ a_{31} & a_{32} & a_{34}-\lambda \end{vmatrix} = 0$$

An example of the change of these constants, indicating the change of stability, during a turning circle manoeuvre, is given in Figure 20.

Concerning the time interval between two steps of the computation, for all manoeuvres ten steps per ship length, based on the initial speed, was applied. The time intervals following from this are given in Table 12.

U_0 m/sec	Δt (sec)	U_0 m/sec	Δt (sec)
8.0	2.7625	4.8	4.6041
6.8	3.2500	3.2	6.9063
5.6	3.9464		
$(U_0\Delta t/L = \cdot 100)$			

Table 12 Time Intervals Applied for Computations

5 Comparison of Computed and Full-Scale Manoeuvres

5.1 Turning Circles

The principal data of the turning circles are summarised in Table 13.

nr.	9A	9B	9D2
δ_0 (degree)	− 34.0	+ 37.0	− 19.0
rpm	100.0	100.0	100.0
U_0 (m/sec)	8.00	8.00	8.00
$\beta(0)$ (degree)	− .358	+ .358	+ .358
$\psi(0)$ (degree)	− .858	+ .758	− .442
$x_0(0)$ (m)	0	− .06	+ .09
$y_0(0)$ (m)	+ .03	+ .03	+ .37
$\dot{\psi}(0)$ (degree/sec)	+ .10	− .20	+ .05
$\dot{\delta}$ (degree/sec)	2.500	2.500	2.500

Table 13 Turning Circle Data

The results of the computed turning circles are shown in Figure B 1 through Figure B 4. As follows from these figures, the (final) rates of turn are somewhat smaller than the full-scale values though, combined with the final speed, the turning diameters agree very well however.

For comparison with the spiral manoeuvre results some additional turning circles have been computed. Only the final values of the various quantities have been used to obtain complete curves.

The computation of the 37 degrees port rudder turning circle has been repeated omitting certain coefficients, which significance was very little, according to the model tests. The results are shown in Figure B 2. As appears from this figure these coefficients have also little importance in the mathematical model.

5.2 Zig-Zag Trials

In Table 14, the principal data of the zig-zag trials are summarised. Concerning the initial conditions, only the course ψ was considered while no other data were available. The values of the rudder rate of turn were derived from the data and figures given by Clarke (1965).

The computed zig-zag manoeuvres are plotted in Figure B 5 through Figure B 12 and compared with the full-scale measurements. The overshoot angles are somewhat smaller, but the mean oscillation periods agree very well. These two quantities are plotted in Figure 22.

Concerning the initial speed conditions of these manoeuvres the adopted linear relation: U_0 = 12.5 x rpm has been applied, while the rpm values for both full-scale trials and computations are the same.

initial conditions				I			II			III			IV			V			VI		
nr.	rpm	U_0 (m/s)	ψ (degr)	$\dot{\delta}$ (degr/sec)	δ_0 (degr)	ψ_{ex} (degr)	$\dot{\delta}$ (degr/sec)	δ_0 (degr)	ψ_{ex} (degr)	$\dot{\delta}$ (degr/sec)	δ_0 (degr)	ψ_{ex} (degr)	$\dot{\delta}$ (degr/sec)	δ_0 (degr)	ψ_{ex} (degr)	$\dot{\delta}$ (degr/sec)	δ_0 (degr)	ψ_{ex} (degr)	$\dot{\delta}$ (degr/sec)	δ_0 (degr)	ψ_{ex} (degr)
7A	97.5	7.80	−2.6	2.708 [1]	19.0	−20.8	3.105	−19.0	14.2	3.850	18.2	−19.6	3.482	−19.2	19.9	3.591	18.6	−18.6	3.482	−19.3	9.5
7C	97.2	7.78	− .4	2.500	8.9	−15.7	2.375	− 9.7	23.2	2.436	8.8	−17.2	2.632	− 9.9	22.4						
7D	98.1	7.85	0	2.982	29.3	−16.9	3.929	−31.0	21.1	4.522	28.5	−16.1	3.719	−31.3	21.5	4.000	29.2	−16.2	3.067	−31.0	2.5
7E	87.0	6.96	0	1.020	9.5	−22.8	1.681	−10.1	23.5	1.887	9.3	−23.0	2.330	−10.3	24.0	1.944	9.3	−17.8	2.143	−10.2	20.0
7F	87.0	6.96	0	2.635	19.1	−16.7	3.565	−19.3	20.7	4.149	18.7	−16.0	3.023	−19.9	16.1	4.115	18.4	−16.2	3.185	−19.4	20.0
7G	86.4	6.91	0	2.305	29.6	−19.5	3.041	−31.3	19.5	4.020	29.2	−19.7	3.400	−30.9	20.1	4.727	28.7	−14.3	3.199	−30.9	20.0
7J	67.5	5.40	− .5	.2.232	18.8	−20.0	2.950	−19.2	19.2	2.875	18.7	−19.8	3.231	−19.5	22.9	2.980	18.8	−19.2	2.760	−19.2	20.0
7L	59.7	4.78	− .7	3.488	29.3	−20.8	4.050	−30.2	19.7	4.997	28.8	−22.0	4.173	−30.5	19.5	4.355	28.8	−20.6	4.539	−30.2	0

[1] The manoeuvres concerned have been computed with the accuracy of these data given here.

Table 14 Zig-Zag Trial Data

6 Final Remarks

To judge the result of the model experiments discussed in this paper, Figure 21 and Figure 22 may serve in the first place. They provide an overall picture of the principal parameters of turning circle, spiral and zig-zag trials:

- Figure 21a, r_c^* against δ_0: relation between turning circle diameter $2/r_c^*$) and rudder angle.
- Figure 21b, U_c against δ_0: final speed reduction of turning circle manoeuvres.
- Figure 22a, t_p against $1/U_0$: relation between oscillation periods of zig-zag trials and initial speed.
- Figure 22b, $\psi_{\max}/\delta_0$ against $1/\delta_0$: relation between overshoot angle and nominal rudder angle.

From these figures, in which the computed quantities are compared with those measured during the full-scale trials, it appears that it is possible to predict the manoeuvring properties of the ship concerned by means of oscillation tests with reasonable accuracy. It must be noted however that both full-scale data and computed data have their uncertainties. In particular this may be important if x_0, y_0 plots are compared, because these plots are obtained very indirectly.

Concerning the zig-zag trials it is found that a little change of the "execution course" has a relatively large effect on the maximum course deviation and the oscillation period. Finally we have to keep in mind that the determination of the manoeuvring properties of a ship via horizontal oscillation tests is rather indirect, at least while the motions of the model during these tests are rather unrealistic. From the four figures above mentioned, it may then be concluded that if scale effects play a role in the present investigation their importance is not very large and of the same magnitude as the accuracy of both the full-scale and model-scale measurements.

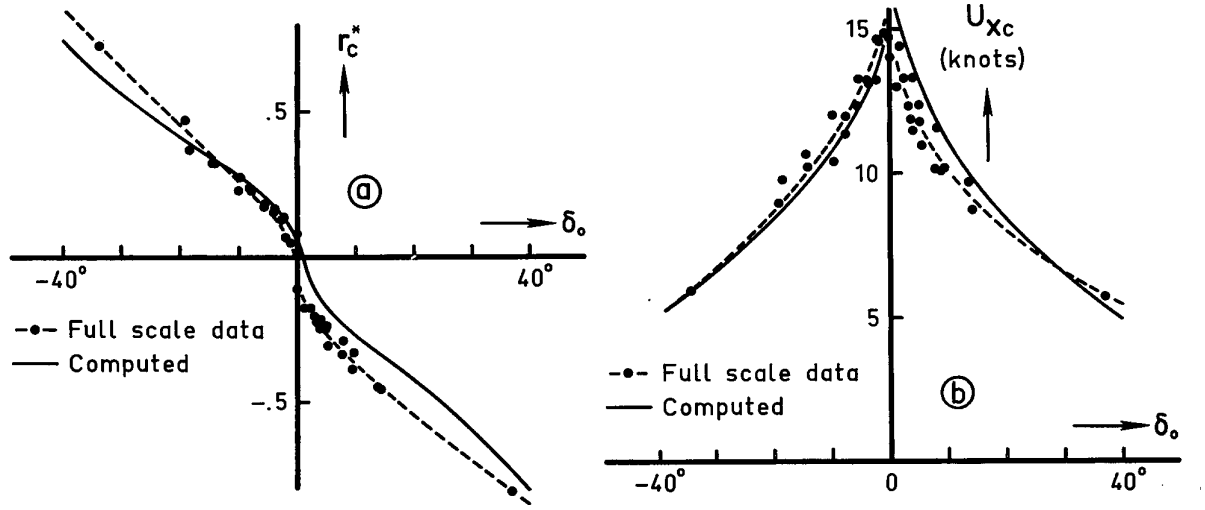

Figure 21 Principal Results of Predicted Circles at 100 Nominal RPM

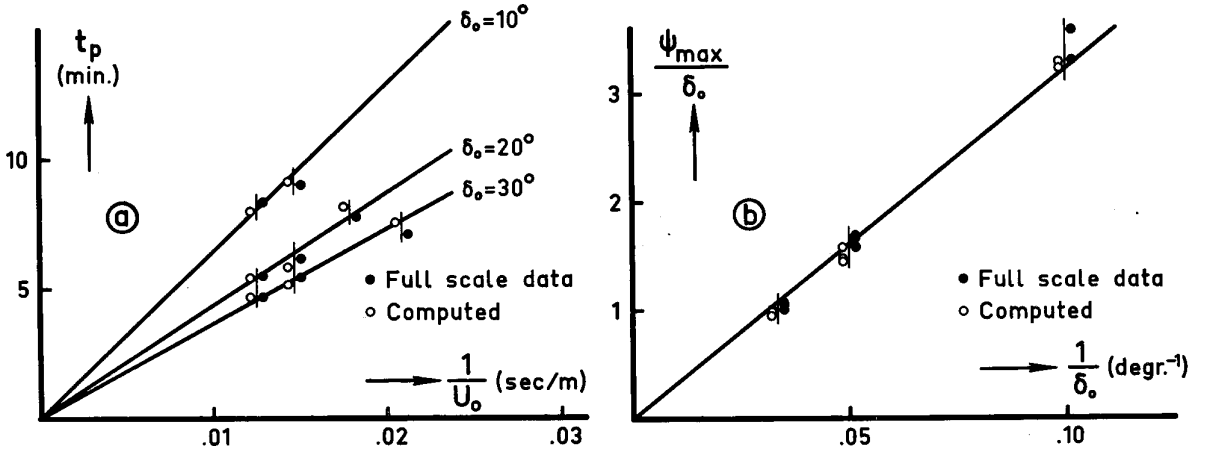

Figure 22 Principal results of Predicted Zig-Zag Tests

7 Recommendations

The mathematical description of the manoeuvring properties is based on a hypothesis, which describes the relation between the forces acting on the ship and the forward speed. The application of this hypothesis is fully justified by the present model experiments. This does not mean however that all hydrodynamic effects, which play a part in this mathematical model, are really necessary for a sufficient description of the horizontal motions. Therefore, it might be interesting to find a simple mathematical model, which properties are not to give and accurate description of the hydrodynamic phenomena but rather of the motions.

8 List of Symbols

m	Mass of the ship
I_{zz}	Moment of inertia of the ship
ρ	Density of water
x_0, y_0	Co-ordinates in space bounded co-ordinate system
Y	Lateral force, positive to starboard
N	Moment around Z_0-axis, positive to the right
X	Longitudinal force
$Y_{\dot{v}}$	Added mass in lateral direction
$N_{\dot{r}}$	Added moment of inertia
$X_{\dot{u}}$	Added mass in longitudinal direction
$Y_{a,1,2}, N_{a,1,2}, X_{1,2,3}$	Components of Y, N and X respectively
$\overline{Y}_2, \overline{N}_2, \overline{X}_2$	Components proportional to $U_R{}^2$
$X_R{}'$	Thrust increment coefficient
$X_R{}^*$	Longitudinal resistance coefficient
$Y_1{}^*$	$= Y_1 / \left(\frac{1}{2} \rho U^2 L^2 \right) \approx Y_1 / \left(\frac{1}{2} \rho U_x{}^2 L^2 \right)$
$N_1{}^*$	$= N_1 / \left(\frac{1}{2} \rho U^2 L^3 \right) \approx N_1 / \left(\frac{1}{2} \rho U_x{}^2 L^3 \right)$
$X_1{}^*$	$= X_1 / \left(\frac{1}{2} \rho U^2 L^2 \right) \approx X_1 / \left(\frac{1}{2} \rho U_x{}^2 L^2 \right)$
U_0	Initial speed
U, $\dot{U}$	Instantaneous forward speed and acceleration (vector)
U_x, $\dot{U}_x$	Instantaneous longitudinal speed and acceleration
U_R	Local velocity near the rudder
v, $\dot{v}$	Sway (drift) velocity and acceleration
r, $\dot{r}$	Yaw angular velocity and acceleration
δ	Rudder angle
u	Speed reduction: $u = U_x - U_0$
v^*	$= v/U = -\sin\beta \approx v/U_x = -\tan\beta$
r^*	$= d\psi / ds^* = L \cdot r / U \approx L / R_r \approx L \cdot r / U_x$
$\dot{v}^*$	$= dv^* / ds^*$
$\dot{r}^*$	$= dr^* / ds^*$
ψ	Heading angle
β	Drift angle
ϕ	Deviation angle
$\dot{\phi}^*$	$= d\phi / ds^* = L/R = L/R_r - L/R_v$
s	Distance covered by the ship
s^*	Distance covered by the ship in ship lengths
R	Radius of curvature

R_v	Drift radius of curvature ($L / R_v = d\beta / ds^*$)
R_r	Yaw radius of curvature ($L / R_r = d\psi / ds^*$)
m'	$= m / 0.5\rho L^3$
I_{zz}'	$= I_{zz} / 0.5\rho \mathrm{L}^5$
v'	$= v / U_0$
r'	$= L \cdot r / U_0$
u'	$= u / U_0$
$\dot{v}'$	$= L \cdot \dot{v} / U_0^2$
$\dot{r}'$	$= L^2 \cdot \dot{r} / U_0^2$
$\dot{u}'$	$= L \cdot \dot{u} / U_0^2$
U_R'	$= U_R / U_0$

9 References

Abkowitz (1964)
M.A. Abkowitz, *Lectures on Ship Hydrodynamics - Steering and Manoeuvrability*, HyA Report HY-5, December 1964.

Clarke (1965)
D. Clarke, *Manoeuvring Trials with the 50.000 Ton Dead-weight Tanker "British Bombardier"*, BSRA Report, December 1965.

Davidson and Schiff (1946)
K.S.M. Davidson and L.J. Schiff, *Turning and Course Keeping Qualities*, SNAME 1946.

Eda and Crane (1962)
H. Eda, and C.L. Crane, *Research on Ship Controllability*, D.L. Report, Stevens Institute of Technology, 1962.

Nomoto (1967)
K. Nomoto, *On the Steering Qualities of Ships*, I.S.P. July 1957.

Van Leeuwen (1964)
G. van Leeuwen, *The Lateral Damping and Added Mass of a Horizontally Oscillating Shipmodel*, T.N.O. Report 65S, December 1964.

Van Leeuwen (1969a)
G. van Leeuwen, *Enkele problemen bij het ontwerpen van een horizontale oscillator (in Dutch)*, T.H. Shipbuilding Laboratory, Report 225, January 1969.

Van Leeuwen (1969b)
Van Leeuwen, *Some Notes on the Discrepancies between the Lateral Motions of Oscillation Tests and Full-Scale Manoeuvres*, T.H. Shipbuilding Laboratory Report 232, April 1969.

Van Leeuwen (1969c)
G. van Leeuwen, *Tentative Results of the Horizontal Oscillation Tests with a 4-Meter Model of the "British Bombardier"*, T.H. Shipbuilding Laboratory, Report 239, June 1969.

Van Leeuwen (1970)
G. van Leeuwen, *A Simplified Non-Linear Model of a Manoeuvring Ship*, T.H. Shipbuilding Laboratory, Report 262, March 1970.

Zunderdorp and Buitenhek (1963)
H.J. Zunderdorp and M. Buitenhek, *Oscillator Techniques at the Shipbuilding Laboratory*, T.H. Shipbuilding Laboratory, Report 111, November 1963.

10 Appendix A

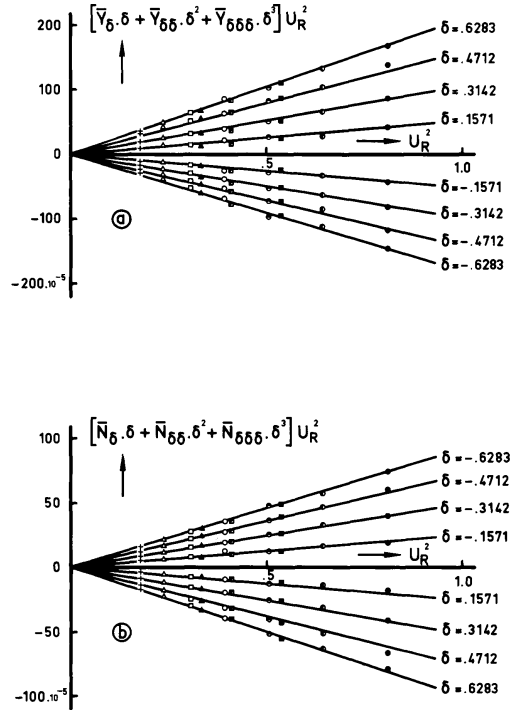

Figure A 1 Lateral Force and Moment due to a Rudder Deflection

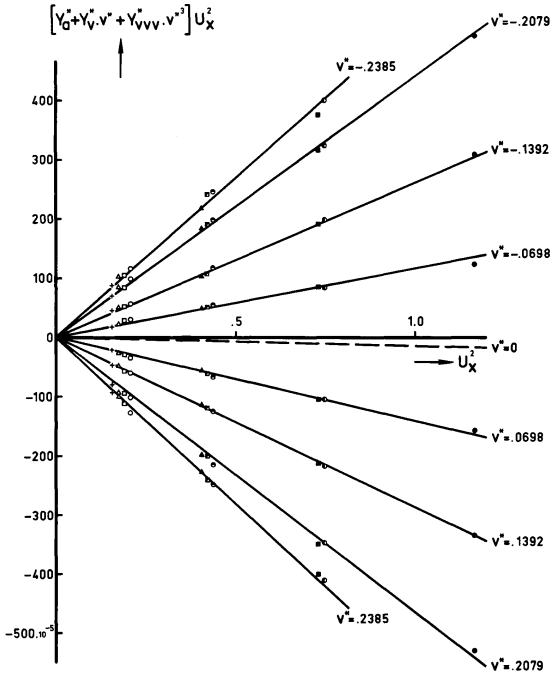

Figure A 2 Lateral Sway Damping Force

U_x(m/sec)	n (r.p.s.)			
1.08	● 12.38			
.86	◐ 11.95	■ 10.29		
.65	◓ 11.54	◪ 9.85	▲ 8.34	
.43	○ 11.20	□ 9.53	△ 8.00	+ 6.50

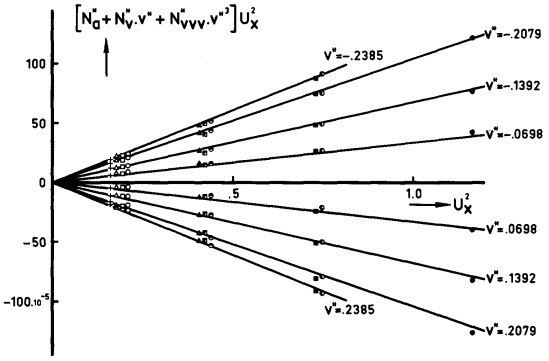

Figure A 3 Lateral Sway Damping Moment

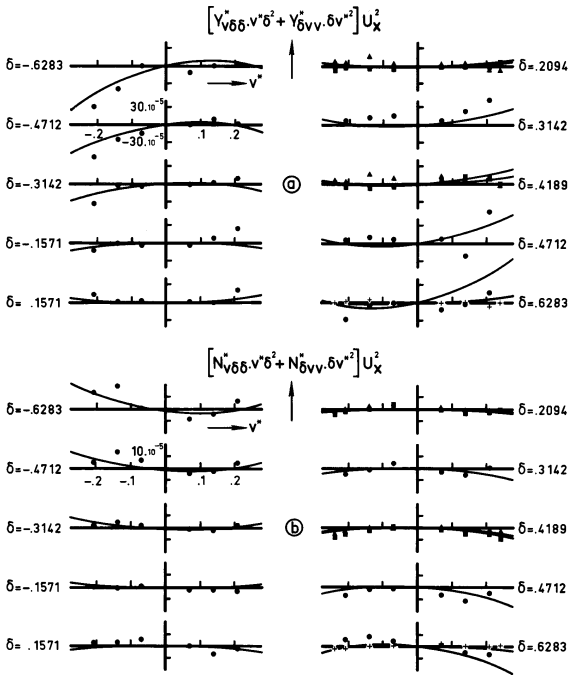

Figure A 4 Rudder Angle – Drift Cross Coupling Effect in Lateral Force and Moment

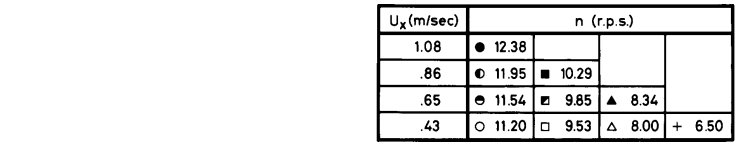

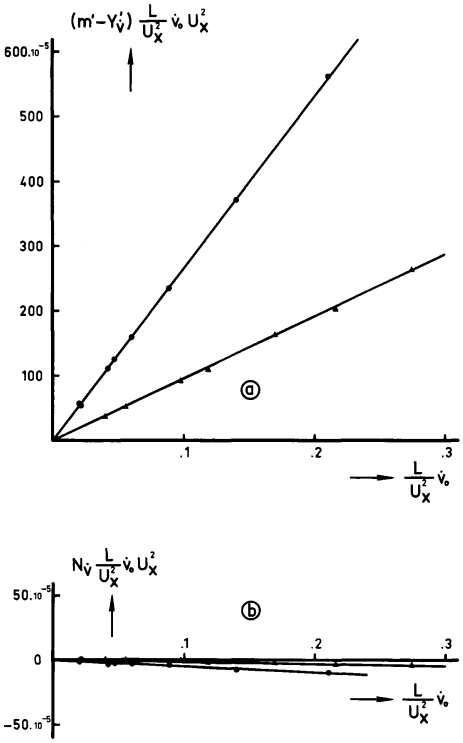

Figure A 5 Swaying Force and Moment due to Lateral Mass

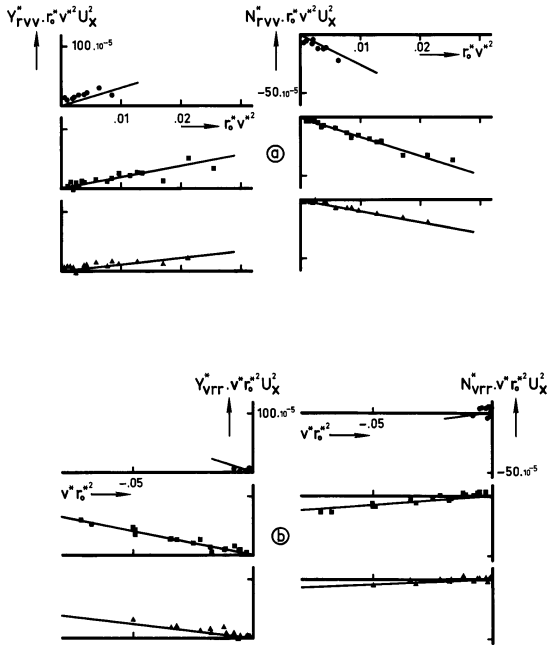

Figure A 7 Yaw Rate – Drift Cross Coupling Effects in Lateral Force and Moment

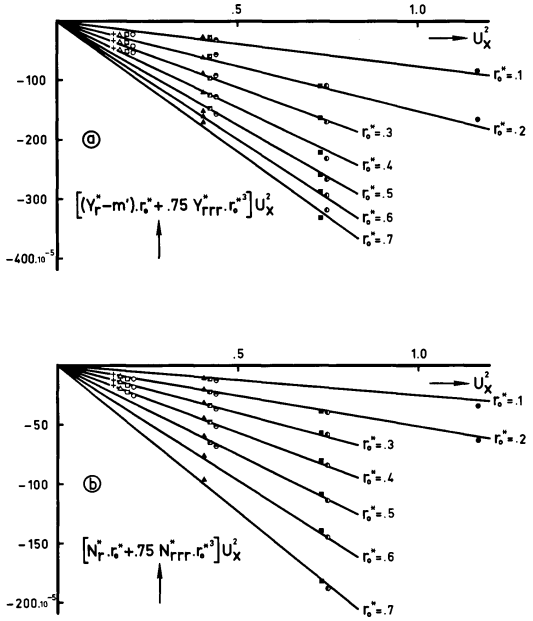

Figure A 6 Lateral Yaw Damping Force and Moment

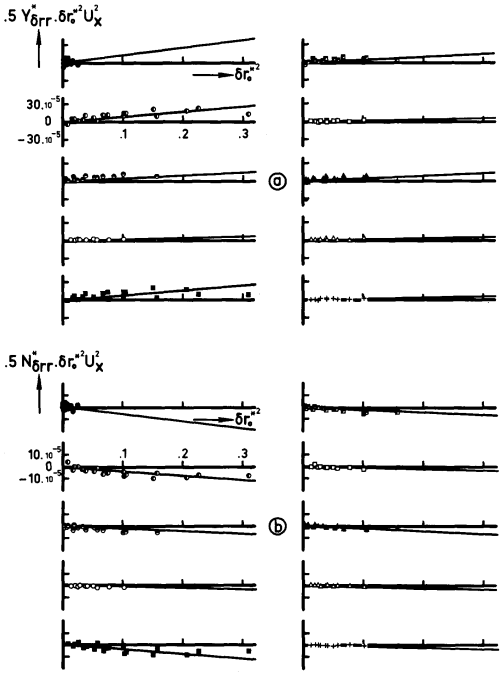

Figure A 8 Rudder Angle – Yaw Rate (δr^2) Cross Coupling Effect in Lateral Force and Moment

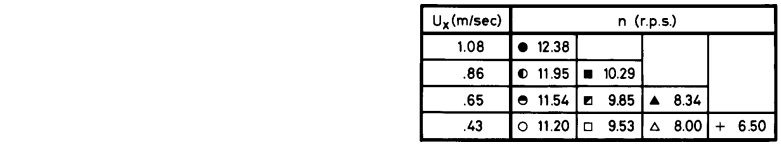

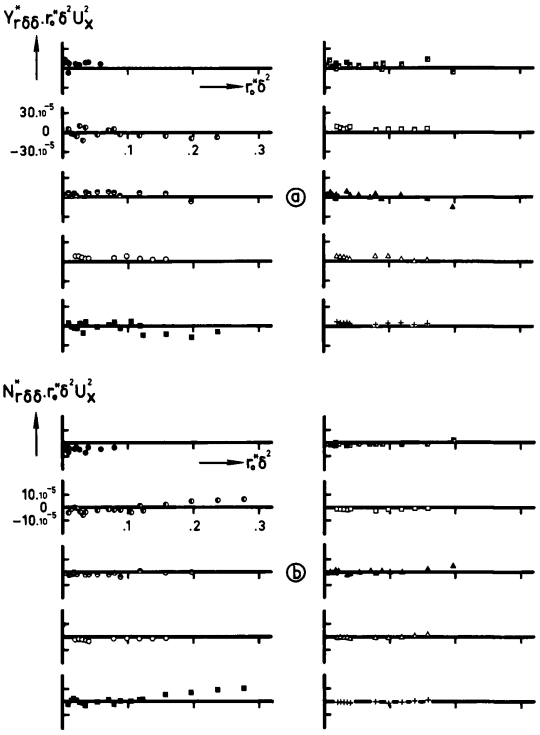

Figure A 9 Yaw Rate – Rudder Angle ($r\delta^2$) Cross Coupling Effect in Lateral Force and Moment

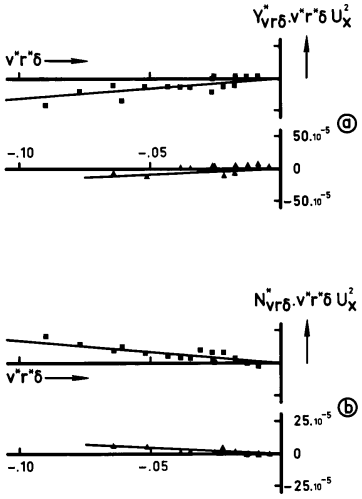

Figure A 10 Drift – Yaw Rate – Rudder Angle Cross Coupling Effect in Lateral Force and Moment

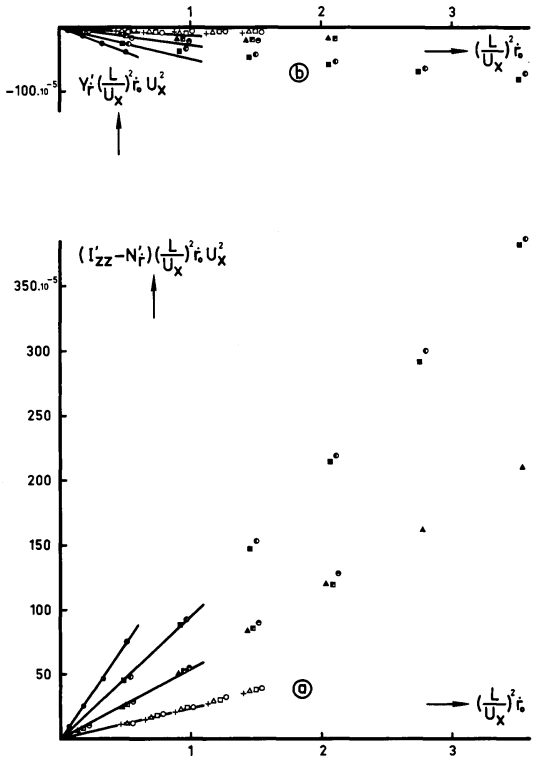

Figure A 11 Yawing Force and Moment due to Moment of Inertia

U_x(m/sec)	n (r.p.s.)				
1.08	● 12.38				
.86	◐ 11.95	■ 10.29			
.65	◓ 11.54	◩ 9.85	▲ 8.34		
.43	○ 11.20	□ 9.53	△ 8.00	+ 6.50	

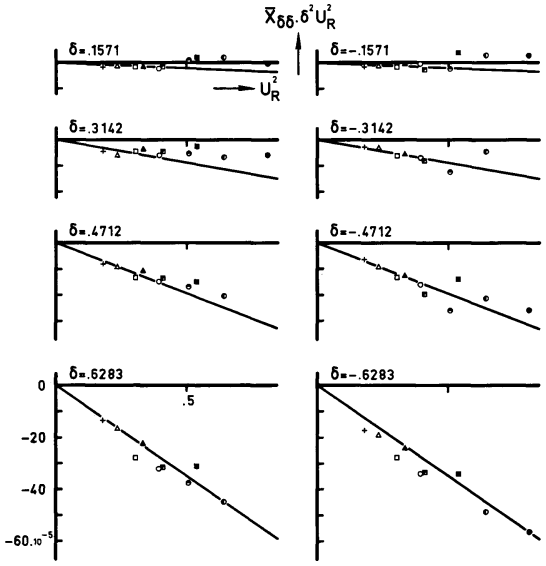

Figure A 12 Longitudinal Force due to a Rudder Deflection

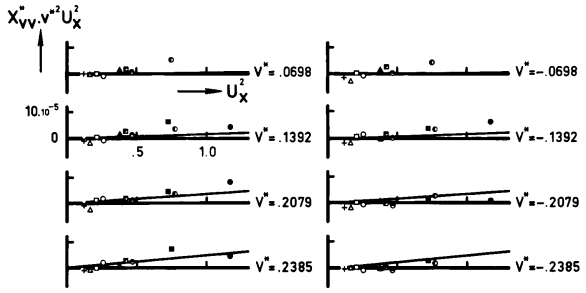

Figure A 13 Longitudinal Sway Damping Force

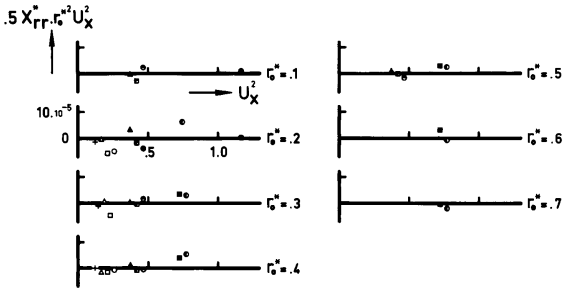

Figure A 14 Longitudinal Yaw Damping Force

U_x(m/sec)	n (r.p.s.)			
1.08	● 12.38			
.86	◐ 11.95	■ 10.29		
.65	◓ 11.54	◪ 9.85	▲ 8.34	
.43	○ 11.20	□ 9.53	△ 8.00	+ 6.50

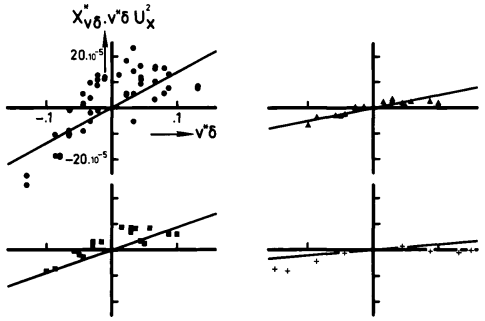

Figure A 15 Rudder Angle – Drift Cross Coupling Effect in Longitudinal Force

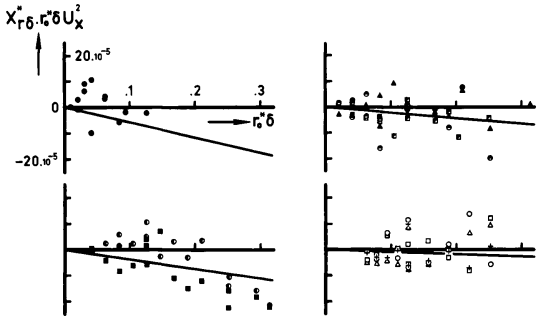

Figure A 16 Rudder angle – Yaw Rate Cross Coupling Effect in Longitudinal Force

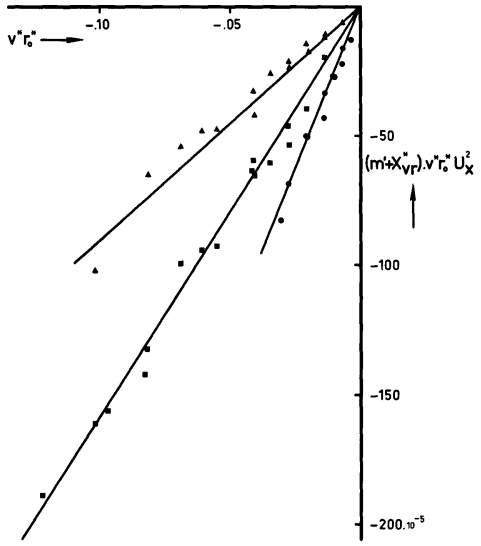

Figure A 17 Longitudinal Force due to Centrifugal Acceleration

SMALL MODEL 1:100

	●	■	▲	+
U_x(m/sec)	.80	.64	.48	.32
n (r.p.s.)	16.43	13.14	9.86	6.57

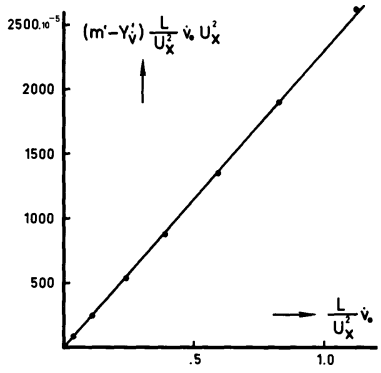

Figure A 18 Swaying Force due to Lateral Mass (Small Model 1:100)

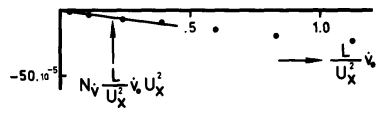

Figure A 19 Swaying Moment due to Lateral Mass (Small Model 1:100)

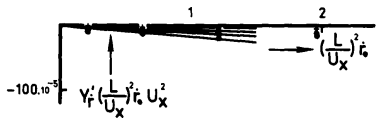

Figure A 20 Yawing Force due to Moment of Inertia (Small Model 1:100)

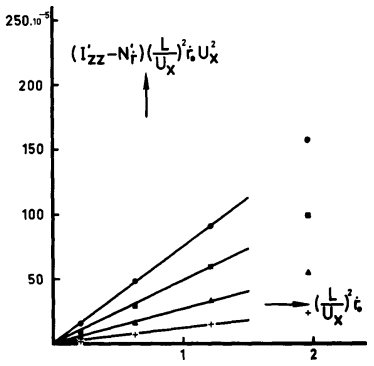

Figure A 21 Yawing Moment due to Moment of Inertia (Small Model 1:100)

SMALL MODEL 1:100

	●	■	▲	+
U_x (m/sec)	.80	.64	.48	.32
n (r.p.s.)	16.43	13.14	9.86	6.57

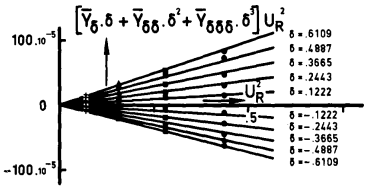

Figure A 22 Lateral Force due to Rudder deflection (Small Model 1:100)

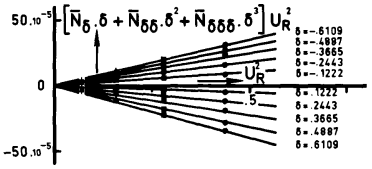

Figure A 23 Lateral Moment due to Rudder Deflection (Small Model 1:100)

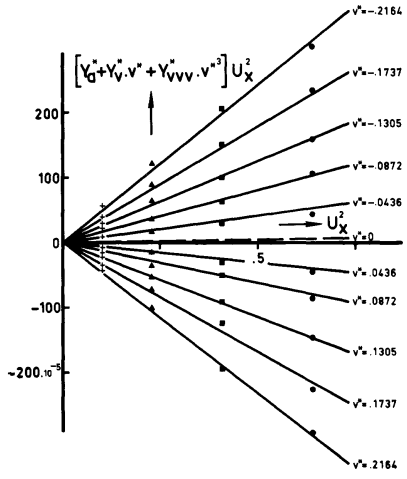

Figure A 24 Lateral sway Damping Force (Small Model 1:100)

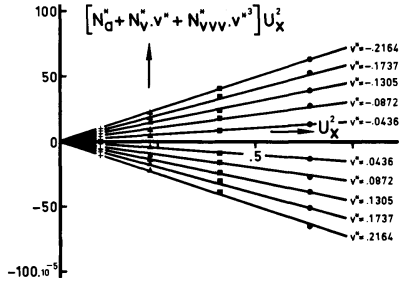

Figure A 25 Lateral Sway Damping Moment (Small Model 1:100)

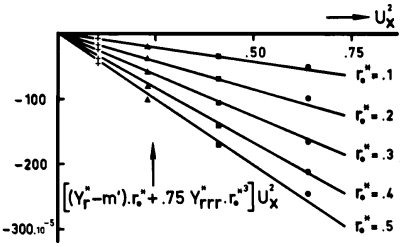

Figure A 26 Lateral Yaw Damping Force (Small Model 1:100)

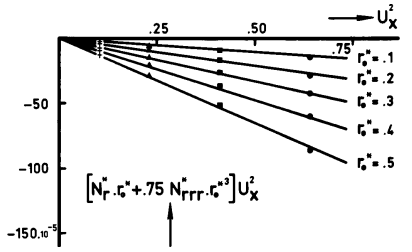

Figure A 27 Lateral Yaw Damping Moment (Small Model 1:100)

11 Appendix B

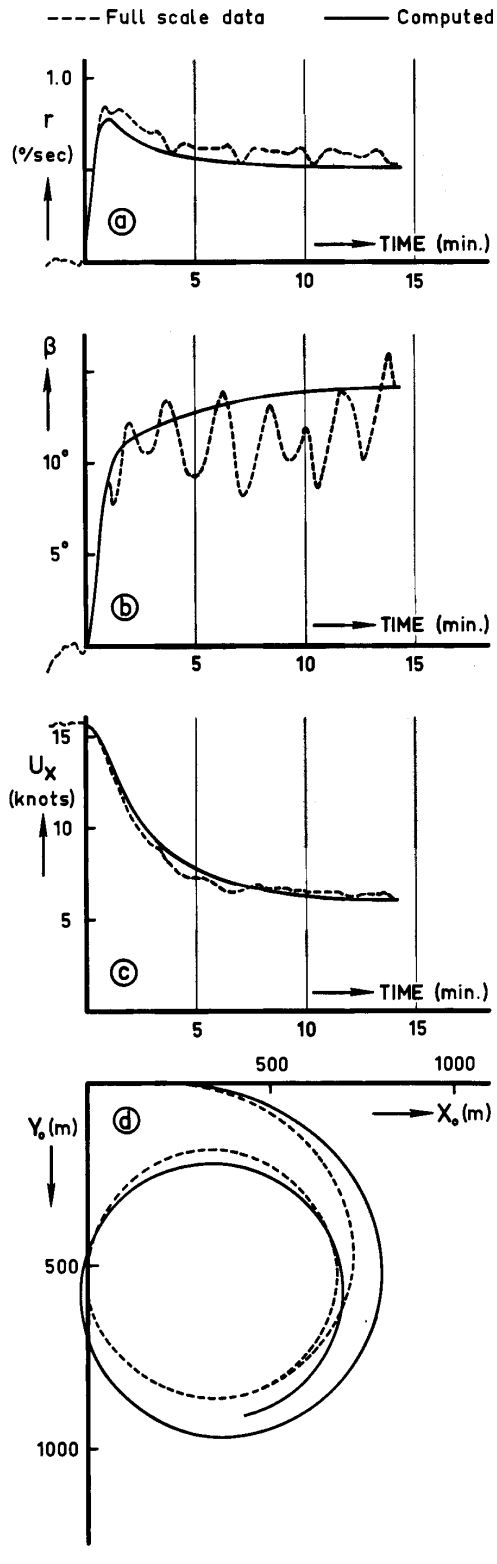

Figure B 1 Time Histories and X-Y Plot of Turning Circle A at 34^0 to Starboard and 100 Nominal RPM

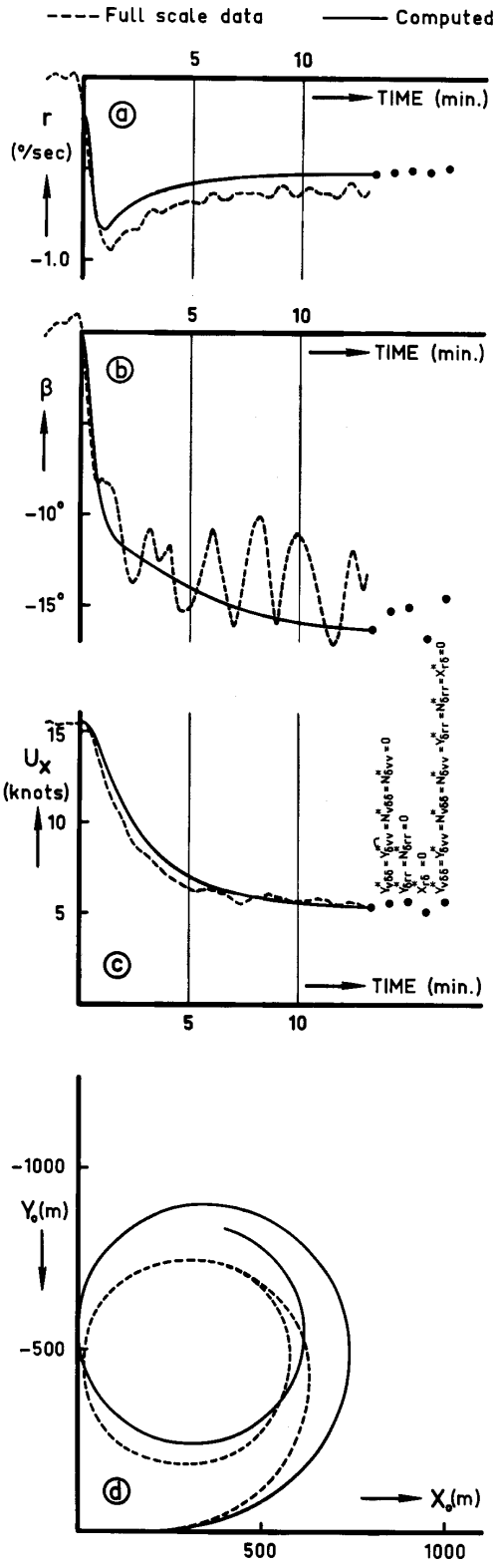

Figure B 2 Time Histories and X-Y Plot of Turning Circle B at 37^0 to Port and 100 Nominal RPM

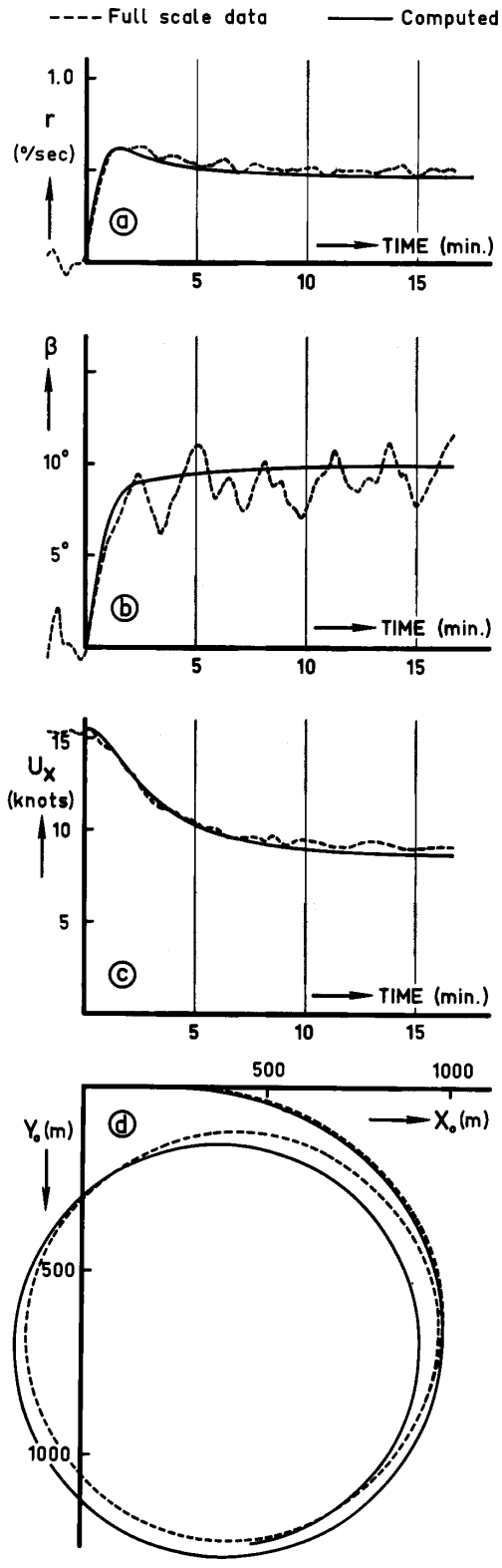

Figure B 3 Time Histories and X-Y Plot of Turning Circle D2 at 19^0 to Starboard and 100 Nominal RPM

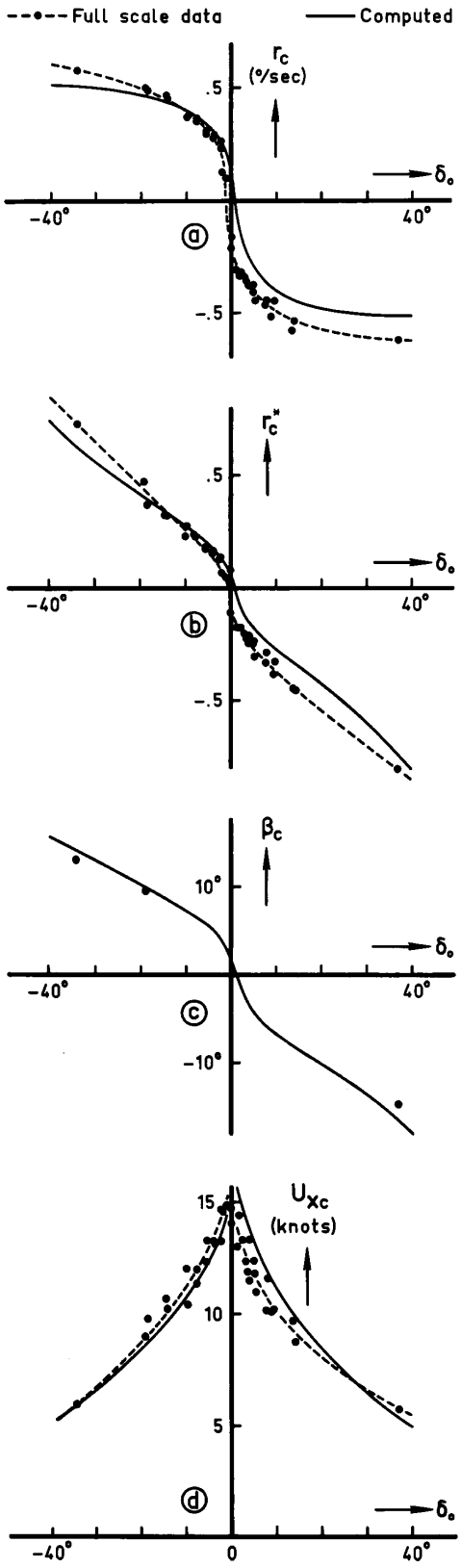

Figure B 4 Turning Circle Characteristics at 100 Nominal RPM

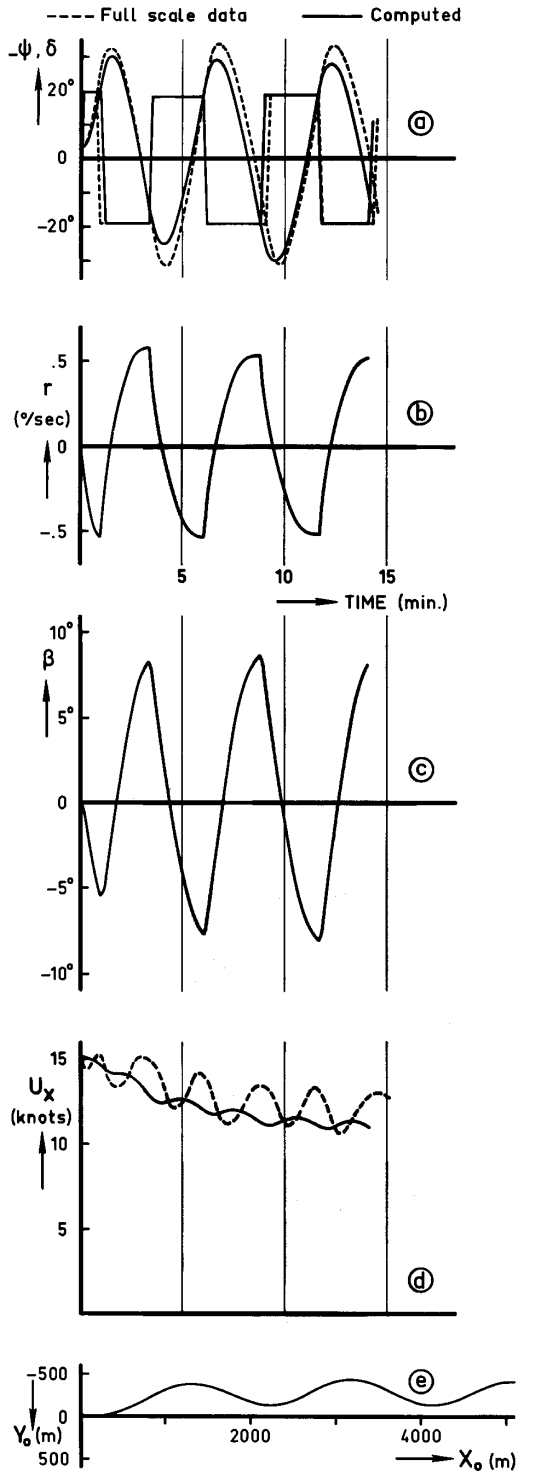

Figure B 5 Time Histories and X-Y Plot of Zig-Zag Test A (20/20) at 100 Nominal RPM

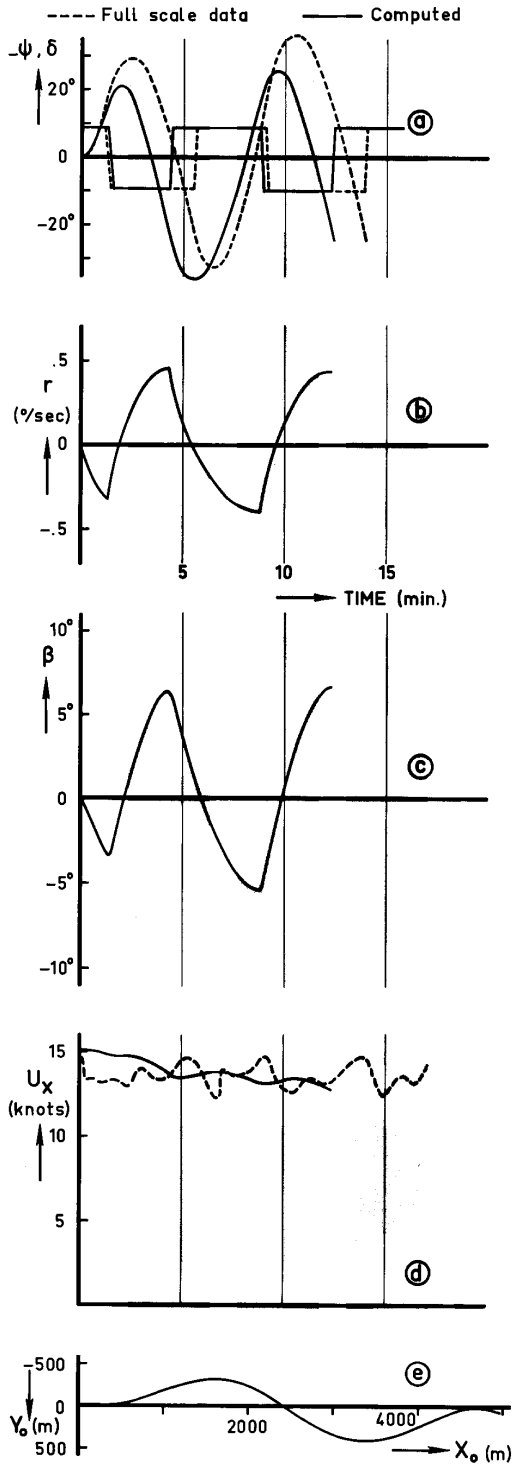

Figure B 6 Time Histories and X-Y Plot of Zig-Zag Test C (10/20) at 100 Nominal RPM

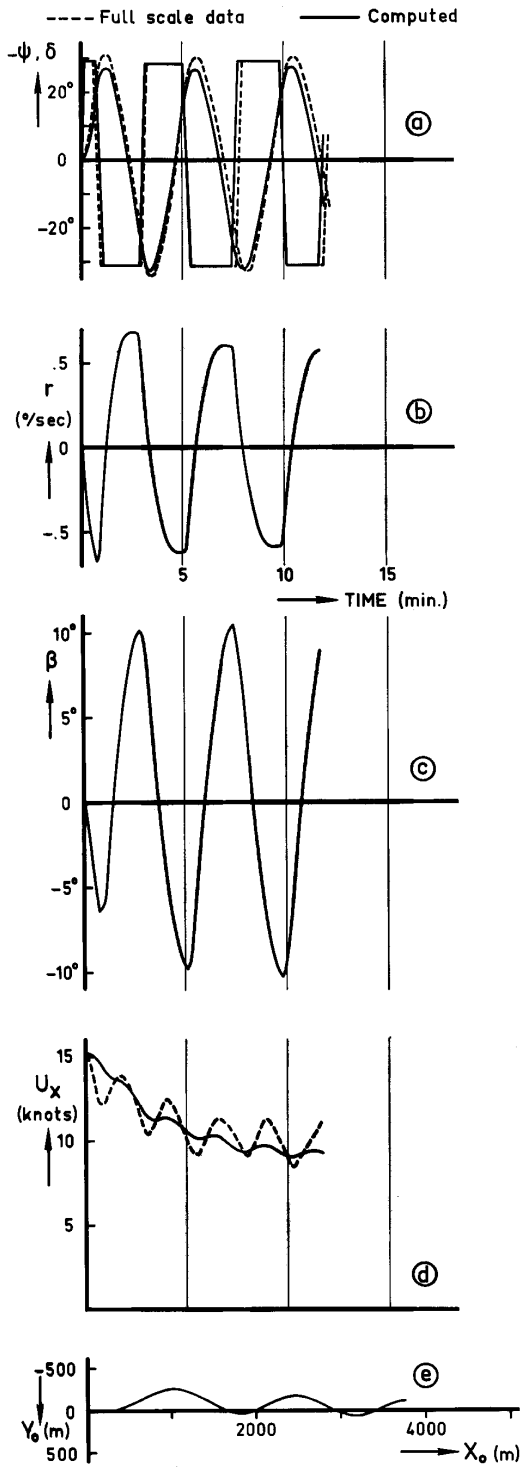

Figure B 7 Time Histories and X-Y Plot of Zig-Zag Test D (30/20) at 100 Nominal RPM

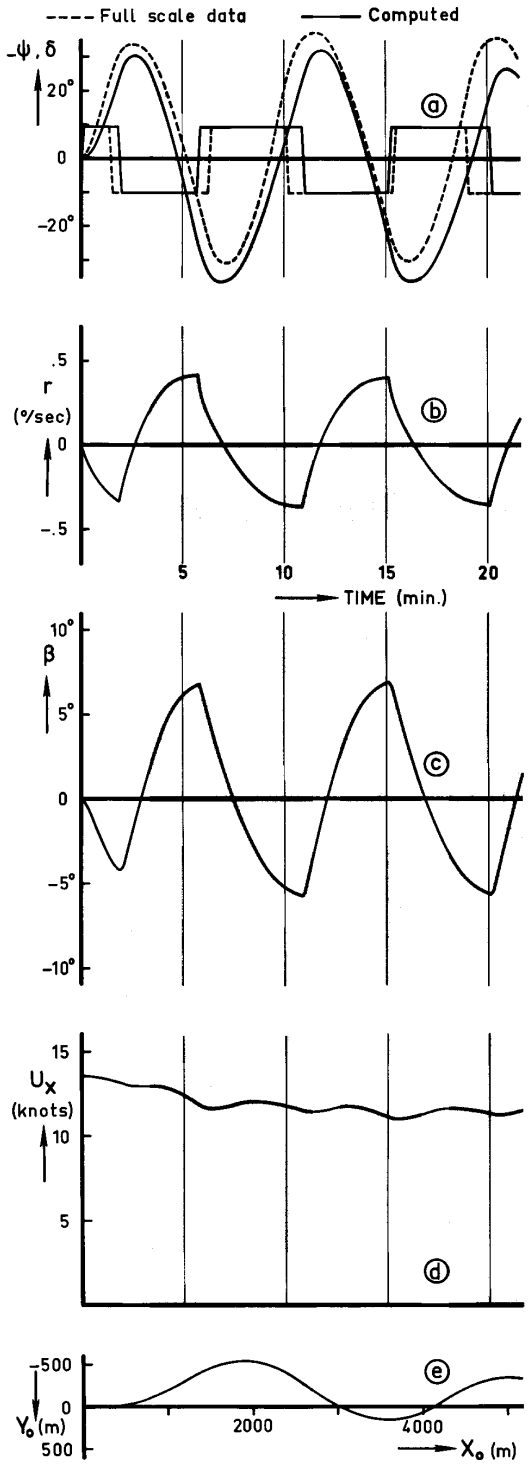

Figure B 8 Time Histories and X-Y Plot of Zig-Zag Test E (10/20) at 85 Nominal RPM

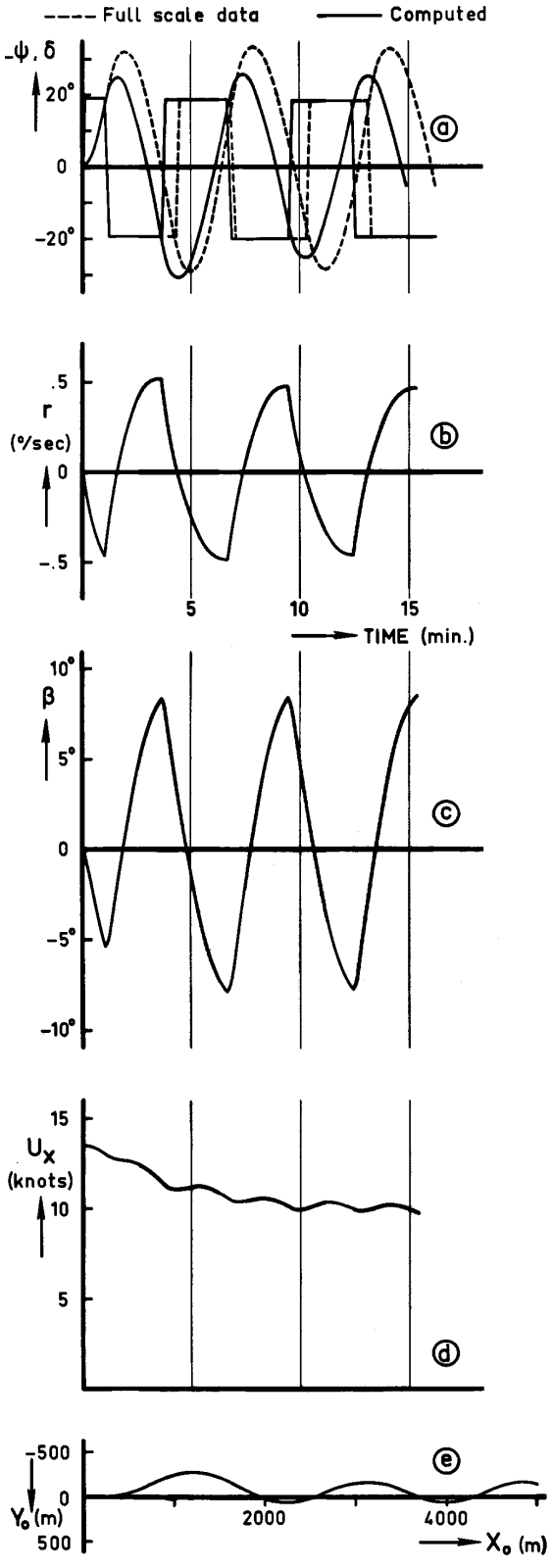

Figure B 9 Time Histories and X-Y Plot of Zig-Zag Test F (20/20) at 85 Nominal RPM

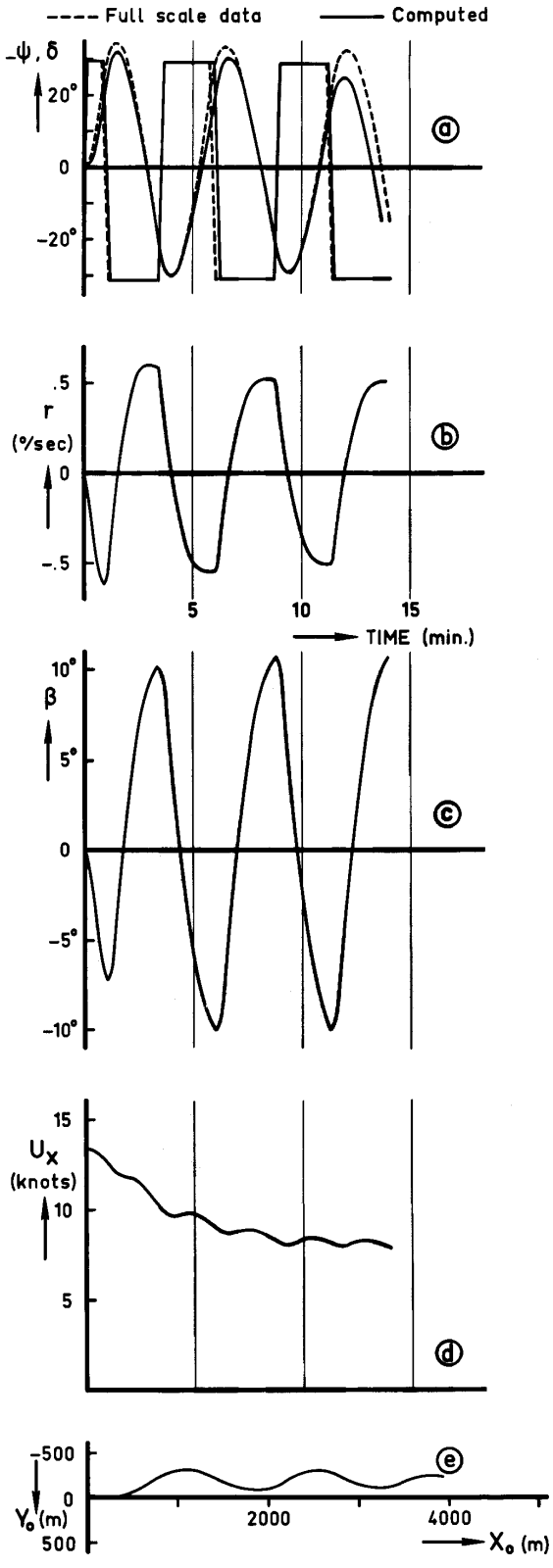

Figure B 10 Time Histories and X-Y Plot of Zig-Zag Test A (30/20) at 85 Nominal RPM

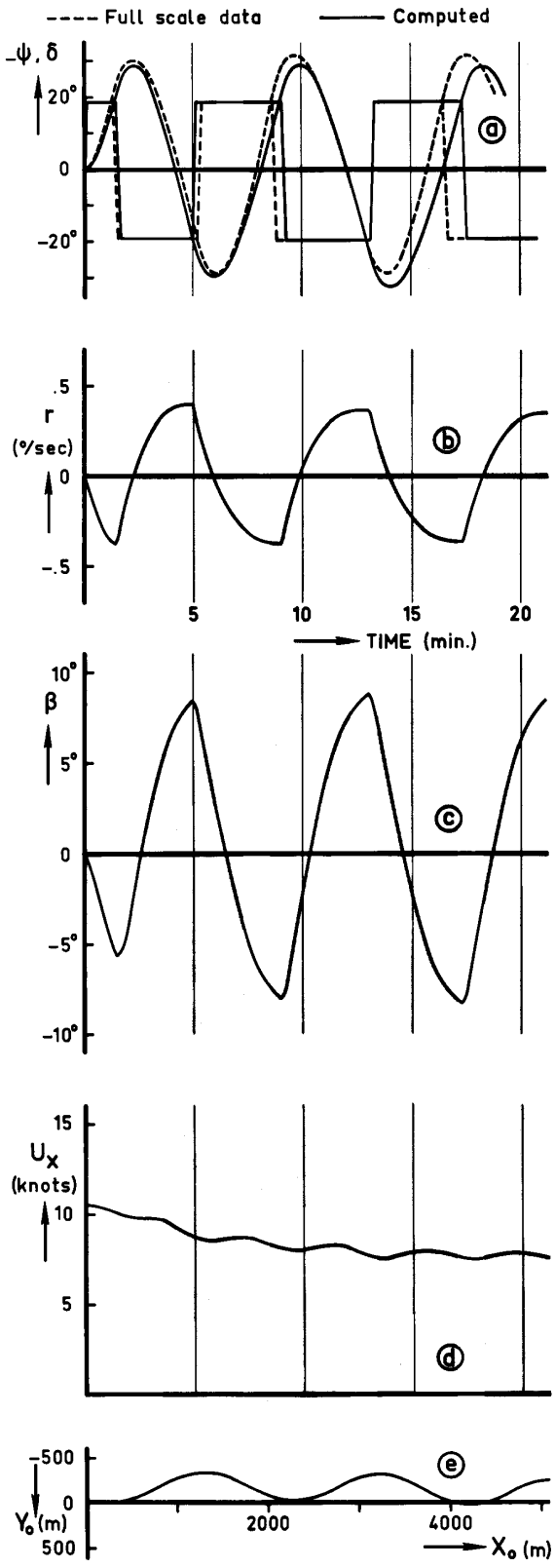

Figure B 11 Time Histories and X-Y Plot of Zig-Zag Test J (20/20) at 70 Nominal RPM

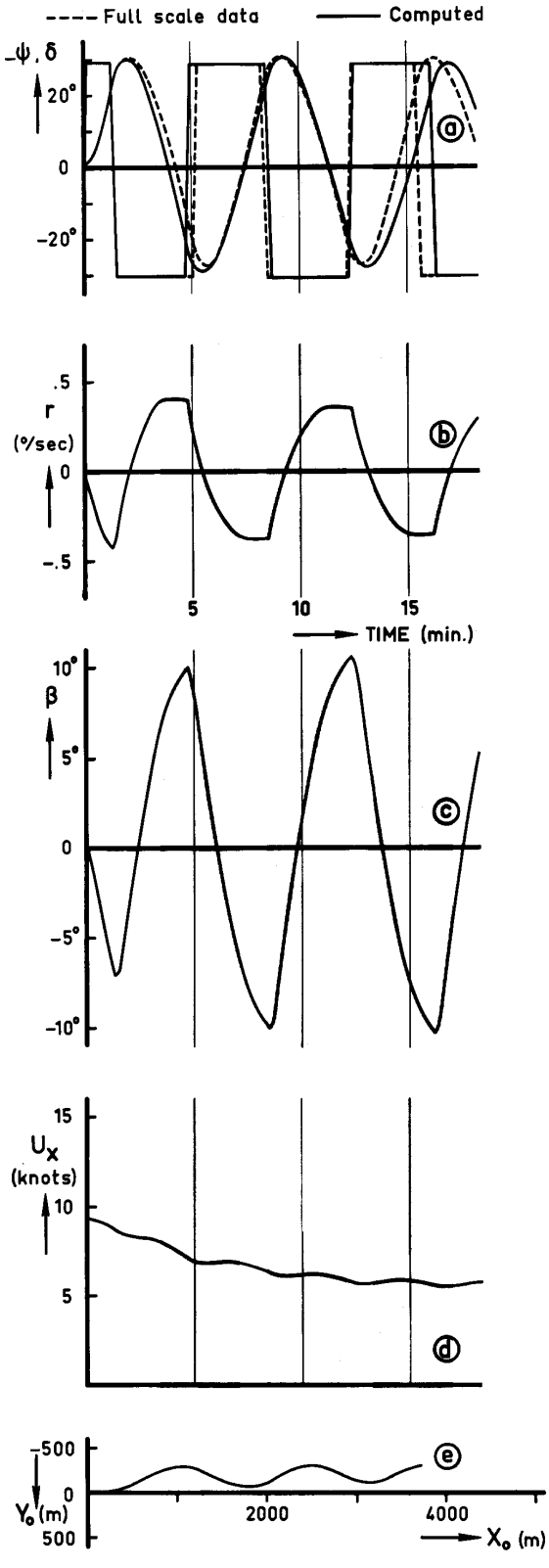

Figure B 12 Time Histories and X-Y Plot of Zig-Zag Test L (30/20) at 60 Nominal RPM